PNL-10744
UC-721

Synthesis, Structural Characterization, and Performance Evaluation of Resorcinol-Formaldehyde (R-F) Ion-Exchange Resin

T. L. Hubler
J. A. Franz
W. J. Shaw
S. A. Bryan
R. T. Hallen
G. N. Brown
L. A. Bray
J. C. Linehan

August 1995

Prepared for
the U.S. Department of Energy
under Contract DE-AC06-76RLO 1830

Pacific Northwest Laboratory
Richland, Washington 99352

DISCLAIMER

Portions of this document may be illegible in electronic image products. Images are produced from the best available original document.

Summary

The 177 underground storage tanks at the U.S. Department of Energy's Hanford Site contain an estimated 180 million tons of high-level radioactive wastes consisting of a mixture of sludge, salt cake, and alkaline supernatant liquids. The insoluble sludge, composed of metal oxides and hydroxides, contains the bulk of most of the radionuclides while the salt cake is composed primarily of sodium salts. The alkaline supernates are concentrated solutions consisting primarily of sodium nitrate and nitrite in which water soluble radionuclides, such as ^{137}Cs, are found.

Economically, it is desirable to remove and concentrate the highly radioactive fraction of the tank wastes for vitrification, with the bulk of the waste being disposed of in a relatively low-cost method. Ion-exchange technology is being evaluated for removal of cesium from waste tanks of both the Hanford and Savannah River Sites.

This report summarizes studies into the synthesis and characterization of resorcinol-formaldehyde (R-F) resin, an organic ion-exchange resin with high selectivity and capacity for the cesium ion, which is a candidate ion-exchange material for use in remediation of tank wastes. The report includes information on the structure/function analysis of R-F resin and the synthetic factors that affect performance of the resin. Some comparison with CS-100, a commercially available phenol-formaldehyde (P-F) resin, and currently the baseline ion-exchanger for removal of cesium ion at Hanford, is made with the R-F resin.

The primary structural unit of the R-F resin was determined to consist of a 1,2,3,4-tetrasubstituted resorcinol ring unit while the CS-100, a P-F resin, was composed mainly of a 1,2,4-trisubstituted ring. The CS-100 resin shows the presence of phenoxy-ether groups. This factor may account for the much lower decontamination factor or performance of CS-100 for cesium ion compared to the R-F resin.

Curing temperatures for the R-F resin were found to be optimal in the range of 105-130 °C. At lower temperatures, insufficient curing, hence crosslinking, of the polymer resin occurs and the selectivity for cesium drops. Curing at elevated temperatures, even under inert atmosphere, leads to chemical degradation of the polymer resin with drastic reduction in performance.

The optimal particle size for R-F resin is in the range of 20-50 mesh-sized particles. Larger particles have lower performance for cesium, due to of particle diffusion limitations. Smaller particles, which have higher surface areas and greater access to ion-exchange sites, probably have lower performance because a large number of the sites are chemically degraded, and are thus not available for ion-exchange.

R-F resin undergoes chemical degradation or oxidation, which destroys ion-exchange sites as correlated with lower cesium K_d's. The ion-exchange sites (hydroxyl groups) are converted to quinones and ketones. CS-100, though it has much lower performance for cesium ion-exchange, is significantly more chemically stable than R-F resin. Exposure to gamma radiation also shows that CS-100 is more radiolytically stable than R-F resin.

Acknowledgments

The authors gratefully acknowledge the data provided for this report from the experiments and analyses conducted by the following staff members: Randy D. Scheele and Richard L. Sell for the thermogravimetric analysis/infrared data; Ronald K. Stephens for the Brunauer, Emmett, Teller analysis; David E. McCready for the x-ray diffraction analysis; Shelley J. Carlson for providing the scanning electron microscopy; and Betty E. Tanaka, Robert J. Elovich, and Jaquetta R. Deschane for performing the K_d analyses.

Acronyms

ASTM - American Society for Testing and Materials

BET - Brunauer, Emmet, Teller

BSC - Boulder Scientific Co.

CP-MAS - cross polarization/magic angle spinning

DOE - U.S. Department of Energy

DSSF - double-shell slurry feed

DTGS - deuterium triglycine sulfate

DVB - divinylbenzene

FID - free induction decay

FTIR - Fourier Transform Infrared

IR - Infrared

K_d - distribution coefficient

NACE - National Association for Corrosion Engineers

NCAW - Neutralized Current Acid Waste

NMR - nuclear magnetic resonance

P-F - phenol-formaldehyde

PNL - Pacific Northwest Laboratory

R-F - resorcinol-formaldehyde

SEM - scanning electron microscopy

TGA/IR - thermogravimetric analysis/infrared

XRD - x-ray diffraction

Contents

Summary iii

Acknowledgments v

Acronyms vii

1.0 Introduction 1-1

2.0 Fundamentals of Organic Ion Exchanger 2-1

2.1 Organic Ion-Exchange Materials 2-1

2.2 Capacity of R-F Resin 2-2

2-3 Selectivity of R-F Resin 2-3

3.0 Experimental 3-1

3.1 Preparation of Resins 3-1

3.1.1 PNL-Synthesized R-F Resin 3-1

3.1.2 Cesium Loading on R-F Resins, Varied Ionic Strength 3-1

3.1.3 Cesium Loading on R-F Resins, Constant Ionic Strength 3-1

3.1.4 Preparation of Acid Form of R-F Resins 3-2

3.1.5 Oxidation of R-F Resins 3-2

3.2 Distribution Coefficient, K_d's 3-2

3.3 Nuclear Magnetic Resonance (NMR) Spectroscopy 3-2

3.3.1 Instrumentation 3-2

3.4 Fourier Transform Infrared Spectroscopy 3-3

3.5 Thermogravimetric/Infrared Analysis, Brunauer, Emmet, Teller Surface Area/Pore Structure Analysis, Scanning Electron Microscopy, and X-Ray Diffraction 3-4

3.6 Radiolytic Stability of R-F and CS-100 Resins 3-4

4.0 Evaluation of CS-100 and R-F Ion Exchange Resins 4-1

4.1 Distribution Coefficients 4-1

4.2 Structural Characterization 4-5

4.2.1 NMR Spectral Characterization of R-F Resin 4-5

4.2.2 Infrared Characterization of R-F Resin 4-9

4.2.3 Additional Structural Characterization of R-F Resin 4-14

4.2.4 Characterization of Cesium-Loaded R-F Resin 4-20

4.3 CS-100 (Phenol-Formaldehyde) Resin 4-26

4.4 Oxidation Studies of R-F and CS-100 Resins 4-28

4.5 Radiolytic Stability of R-F and CS-100 Resins 4-32

4.5.1 Gas Generation for Cation Exchange Resin and NCAW Supernate 4-41

4.5.2 Corrosion 4-45

5.0 Conclusion/Recommendations 5-1

6.0 References 6-1

Figures

2-1 Addition-type Polymer Resin Prepared from Styrene and Divinylbenzene (DVB) 2-1

2-2 Condensation-type Polymer Made from Phenol and Formaldehyde 2-2

2-3 Ring Numbering Scheme for Resorcinol 2-2

2-4 Acid/Base Equilibria of Diprotic Resorcinol 2-3

2-5 The Relationship Between (A) Swelling and (B) Contracting Due to the Selectivity Observed for Phenolic Condensation Polymers 2-6

4-1 C-undecylcalix-[4]-resorcinarene (R = undecyl) 4-5

4-2 Model Structures Used to Calculate ^{13}C NMR Chemical Shifts for A) 1,2,4,5- and B) 1,2,3,4-tetrasubstituted Resorcinol Rings 4-6

4-3 ^{13}C NMR of Resorcinol-Formaldehyde Resin (2-A) 4-7

4-4 ^{13}C NMR of C-undecylcalix-[4]-resorcinarene 4-7

4-5 ^{13}C NMR of R-F Resin Prepared with ^{13}C-Labeled Formaldehyde 4-8

4-6 ^{13}C NMR Spectra of R-F Resin Prepared with ^{13}C-Labeled Methanol 4-9

4-7 ^{13}C NMR of BSC-210 in Different Ionic Forms 4-10

4-8 Infrared Spectrum for Resorcinol, KBr Pellet 4-11

4-9 Infrared Spectrum for C-undecylcalix[4]resorcinarene Monohydrate, KBr Pellet 4-11

4-10 Infrared Spectrum of R-F Resin 55197-1-A, KBr Pellet 4-13

4-11 Photomicrographs of BSC-187 R-F Resin Used for IR Analysis (top) and of PNL-Synthesized R-F Resin 55197-2-A, Showing 20 to 50 Mesh Particles (bottom) 4-15

4-12 Infrared Spectra of BSC-187 R-F Resin 4-17

4-13 SEM Photomicrographs of PNL-Synthesized R-F Resin at (i) 100 um, (ii) 50 um, (iii) 20 um, and (iv) 50 um Magnification 4-19

4-14 ^{133}Cs NMR Spectra of BSC-210 Contacted with Varied Ionic Strength CsOH Solutions 4-22

4-15 ^{13}C NMR of BSC-210 Contacted with Varied Ionic Strengths of CsOH Solutions 4-23

4-16 ^{13}C NMR of BSC-210 Contacted with Constant Ionic Strength Na^+/Cs^+ Solutions 4-24

4-17 ^{133}Cs NMR Spectra of Constant Ionic Strength Na^+/Cs^+ Solutions 4-25

4-18 ^{13}C NMR of CS-100 in Na^+ and H^+ Forms 4-27

4-19 The Two Structural Components of Duolite CS-100 Resin: A - 54.8%; B - 45.2% 4-28

4-20 ^{13}C NMR of (a) BSC-187 (K^+ Form, Dry) as Received (b) BSC-187 After Being Contacted for Six Months with 2M NaOH in the Presence of Air 4-29

4-21 Oxidation Kinetics of R-F and CS-100 Resins in Aqueous Media 4-30

4-22 ^{13}C NMR BSC-210 (a) Before with Alkaline Solution (b) After Being Contacted with 1M NaOH for 70 h Under Air Purge 4-31

4-23 ^{13}C NMR Spectra of BSC-210 Resin Obtained at 12 kHz MAS for Conditions of No Gamma Irradiation with Flowing NCAW Waste Simulant (top) Compared to Standard BSC-210 Resin (bottom) 4-33

4-24 ^{13}C NMR Spectra of BSC-210 Resin Obtained at 12 kHz MAS for Conditions of Gamma Irradiation (1×10^9 R) with Flowing NCAW Waste Simulant (top) Compared to Standard BSC-210 Resin (bottom) 4-34

4-25 ^{13}C NMR Spectra of BSC-210 Resin Obtained at 12 kHz MAS for Conditions of Gamma Irradiation (1×10^9 R) with Static NCAW Waste Simulant (top) Compared to Standard BSC-210 Resin (bottom) 4-35

4-26 ^{13}C NMR Spectra of BSC-210 Resin Obtained at 12 kHz MAS for Conditions of No Gamma Irradiation with Static NCAW Waste Simulant (top) Compared to Standard BSC-210 Resin (bottom) 4-36

4-27 ^{13}C NMR Spectra of CS-100 Resin Obtained at 12 kHz MAS for Conditions of No Gamma Irradiation with Flowing NCAW Waste Simulant (top) Compared to Standard CS-100 Resin (bottom) 4-37

4-28 ^{13}C NMR Spectra of CS-100 Resin Obtained at 12 kHz MAS for Conditions of Gamma Irradiation (5×10^8 R) with Flowing NCAW Waste Simulant (top) Compared to Standard CS-100 Resin (bottom) 4-38

4-29 ^{13}C NMR Spectra of CS-100 Resin Obtained at 12 kHz MAS for Conditions of Gamma Irradiation (5×10^8 R) with Static NCAW Waste Simulant (top) Compared to Standard CS-100 Resin (bottom) 4-39

4-30 ^{13}C NMR Spectra of CS-100 Resin Obtained at 12 kHz MAS for Conditions of No Gamma Irradiation with Static NCAW Waste Simulant (top) Compared to Standard CS-100 Resin (bottom) 4-40

4-31 Gas Generation from BSC-187 R-F Resin in NCAW Supernate Under Gamma Irradiation and Control Conditions 4-42

4-32 Gas Generation from BSC-210 R-F Resin in NCAW Supernate Under Gamma Irradiation and Control Conditions 4-42

4-33 Gas Generation from CS-100 Resin in NCAW Supernate Under Gamma Irradiation and Control Conditions 4-43

4-34 Comparison of Oxygen Gas Generation from CS-100, BSC-187, and BSC-210 Resins in NCAW Supernate Under Gamma Irradiation and Control Conditions 4-43

4-35 Gas Generation from NCAW Supernate Under Gamma Irradiation 4-44

Tables

3-1 DSSF Simulant Composition 3-3

4-1 Distribution Coefficients for Resorcinol-Formaldehyde Ion-Exchange Resins 4-2

4-2 Effect of Temperature on Distribution Coefficients for Resin 55197-2-B 4-4

4-3 Effect of Particle Size on Distribution Coefficients for Resin 55197-15-C 4-4

4-4 Bands and Assignments for the IR Spectrum of Resorcinol 4-12

4-5 Bands and Assignments for the IR Spectrum of R-F Resin 55197-1-A 4-13

4-6 Elemental Analyses for BSC-187 in H^+, Na^+, K^+, and Cs^+ Forms 4-18

4-7 Elemental Analyses for Cesium-Loaded BSC-210 Resin Obtained from Contact with Various Ionic-Strength CsOH Solutions 4-20

4-8 Elemental Analyses of BSC-210 Contacted with Solutions of Constant 2M OH- Ionic Strength, but Varying Na^+/Cs^+ Ratios 4-26

4-9 Elemental Analyses of CS-100 in H^+ and Na^+ Ionic Forms 4-26

4-10 Elemental Analyses of BSC-210 Resin Purged with Air for Varied Lengths of Time 4-32

4-11 G Values for the Production of Gases for Several NCAW-Simulated Waste Supernate Solutions Containing R-F Resins, CS-100 Resin, and NCAW Supernate Only 4-41

4-12 Coupon Corrosion Test Summary for CS-100 and R-F Resins 4-46

1.0 Introduction

The U.S. Department of Energy's (DOE) Hanford Site, located in southeastern Washington State, occupies an area of 560 square miles and was established in 1944 to produce plutonium for the U.S. defense mission. Over the course of decades, hazardous, toxic, and radioactive chemical wastes were generated and disposed of in a variety of ways including storage in underground tanks. An estimated 180 million tons of high-level radioactive wastes are stored in 177 underground storage tanks. During production of fissile plutonium, large quantities of ^{90}Sr and ^{137}Cs were produced. The high abundance and intermediate length half-lives of these fission products are the reason that effort is directed toward selective removal of these radionuclides from the bulk waste stream before final tank waste disposal is effected. Economically, it is desirable to remove the highly radioactive fraction of the tank waste for vitrification, with the bulk of the waste disposed in a relatively low-cost method. Ion-exchange technology is being evaluated for removing cesium from Hanford Site waste tanks. This report presents studies into the synthesis and characterization of resorcinol-formaldehyde (R-F) resin, an organic ion-exchange resin with high selectivity and capacity for cesium ions. R-F resin is being considered for use in removing cesium from alkaline tank waste supernates.

The objectives of this report are to provide baseline information about the primary structure and stability of R-F resin as an aid for evaluating its potential as a cesium-selective ion-exchange resin. Specifically, this work was directed toward

- establishing methods for determining the structure of R-F resin
- determining baseline structural data typical of R-F resin
- examining and identifying synthetic factors affecting resin performance
- correlating spectroscopic information with performance data to establish structure/function relationships
- using nuclear magnetic resonance (NMR) spectroscopy to obtain information about the ion-exchange sites in the R-F resin.

This report summarizes data and analyses performed by Pacific Northwest Laboratory (PNL)[a] on the structural characterization of R-F resin and provides some comparison to Duolite CS-100, a commercially available organic ion-exchange resin. This report is not all inclusive and research on the fundamental chemistry of the R-F resin is continuing.

The experimental approach used to characterize R-F resin was conducted using primarily two types of data: batch distribution coefficients (K_d's) and solid-state ^{13}C NMR. Comparison of these data for a particular resin allowed correlation of resin performance to resin structure. Additional characterization techniques included solid-state ^{133}Cs NMR, elemental analyses, thermogravimetric analysis/infrared (TGA/IR), Brunauer, Emmett, Teller (BET) surface area/pore structure analysis, and scanning electron microscope (SEM).

The approach used to determine the basic structure of the R-F polymer resin was to examine the solid-state ^{13}C NMR spectra for R-F resin and to prepare selectively labeled ^{13}C enriched resin samples to correlate the fate of the chemical reagents with their functionality in the resin product. Additionally,

[a] The Pacific Northwest Laboratory is operated for the U.S. Department of Energy by Battelle Memorial Institute under Contract DE-AC06-76RLO 1830.

^{133}Cs NMR was used to characterize samples of R-F resin that were loaded with varying amounts of cesium ion to give insight into the nature of the ion-exchange site and the environment presented to the cesium ion. IR analysis of resin samples gave basic structural information about the resin by a qualitative assessment of the functional group absorptions found in the spectra.

Analysis of the K_d's obtained for various samples correlated performance of the resins with their structure and were used to gauge the effects of synthetic variables encountered during the preparation of R-F resin. A few synthetic factors, which were correlated to resin performance, were curing temperature and particle size. Another important area of investigation into resin structure/function was that of the chemical and radiolytic stability of the resin, which was addressed by comparison of K_d's with ^{13}C NMR spectra.

2.0 Fundamentals of Organic Ion-Exchanger

2.1 Organic Ion-Exchange Materials

Organic-based ion-exchange materials can be divided into two primary classes: Addition-type polymer resins and condensation-type polymers. By inclusion of the proper chemical functionality, both classes of materials can be used to design ion-exchange materials for either cations or anions. For this discussion, only the cation exchangers were considered.

The first and most prevalent class of organic ion-exchangers are addition-type polymer resins, the typical example being styrene-divinylbenzene (DVB) class of materials (Figure 2-1). An important property of this class of materials is that the amount of crosslinking of the polymer can be accurately controlled by the ratios of styrene to DVB used. Resins with low DVB content are soft and gelatinous and swell strongly, while those with higher DVB content are mechanically more stable and swell very little. The ion-exchange groups in these resins are introduced after polymerization. Commonly, sulfonation of the aromatic rings is used as the ion-exchange functionality. These highly crosslinked resins are macroreticular, i.e., they have high surface area and large pore structure.

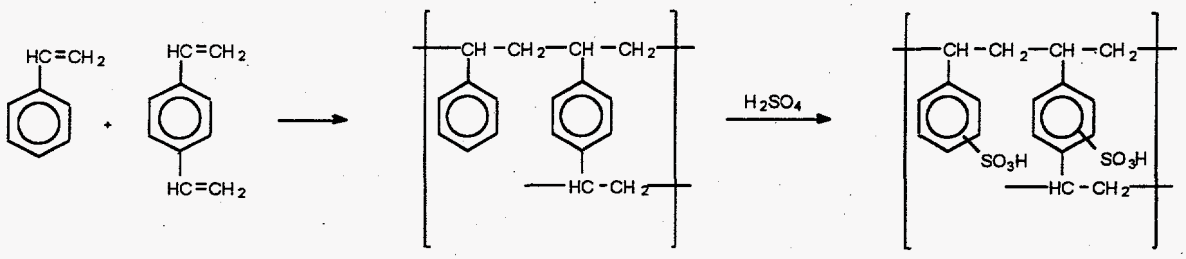

Figure 2-1. Addition-type Polymer Resin Prepared from Styrene and Divinylbenzene (DVB)

The second class of organic ion-exchange materials are condensation-type polymers, as exemplified by phenol-formaldehyde (P-F) and R-F resin (Figure 2-2). These polymer resins are prepared by condensation of the aldehyde with the phenolic ring under alkaline conditions. The fixed-ionic groups in these resins are the ring hydroxyl groups, which can be used for ion-exchange only at higher pH regimes due to the high pK_a of the phenolic -OH group. Introduction of other functional groups such as carboxylic acids and sulfonic acid groups, which have a higher acid strength, make operation of ion-exchange at a lower pH possible for these resins. These resins are heterogeneous microreticular resins, which are composed of highly crosslinked "islands" embedded in regions of lower crosslinking [1].

For both addition and condensation type polymers, it is possible to prepare resins that have chelating groups (e.g., iminodiacetic acid groups), which are amphoteric ion-exchange groups. These resins are generally used for ion-exchange of the transition metals. Other ion-exchange resins have crown ethers incorporated into the resin matrix [2]. In general, for the crown ether resins, ion-exchange does not occur per se, but rather complexation. This means that both the cation (usually alkali, alkaline earth) and anion are absorbed into the exchanger together. Separations can usually be completed

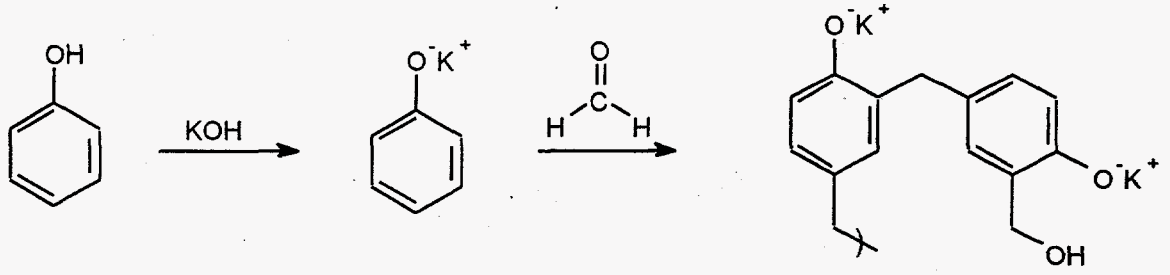

Figure 2-2. Condensation-type Polymer Made from Phenol and Formaldehyde

chromatographically by using water as the eluent. For all of the aforementioned resins, it should be noted that the fixed ionic class can also be located on an alkyl sidechain and is not confined to a position on an aromatic ring.

2.2 Capacity of R-F Resin

The theoretical maximum capacity of R-F resin can be calculated based on the number of fixed ionic groups and is usually expressed in terms of a weight capacity with units of meq/g. The resorcinol ring (Figure 2-3) has two fixed-ionic (hydroxyl) groups in the 1 and 3 positions of the ring. Calculation of the theoretical maximum capacity for R-F resin gives a value of 15.6 to 16.5 meq/g depending on the number of crosslinking methylene groups attached to each ring unit. As will be seen in the discussion of the resin structure, there are an average of two methylene groups per polymer unit; therefore, the theoretical maximum capacity of the R-F resin is 16.5 meq/g.

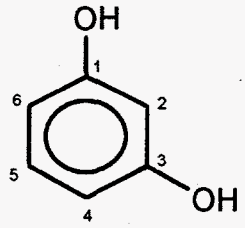

Figure 2-3. Ring Numbering Scheme for Resorcinol

The effective capacity observed for a resin depends upon the experimental conditions used to make the determination, especially for the case of weak acid strength resins. It is essential that operation of ion-exchange processes are carried out under appropriate pH conditions. For example, the weak acid R-F resin is primarily nonionic at low pH, and does not undergo significant ion-exchange at low pH (strong

acid resins are nearly completely ionized under any conditions). The two stepwise pK_a's for the resorcinol hydroxyl groups occur at 9.2 and 11.3 [3] as shown in Figure 2-4. Therefore, maximum use of R-F resin exchange site capacity occurs only at an approximate pH of 12 and above where both hydroxyl groups for each ring unit are theoretically deprotonated and are available for ion-exchange.

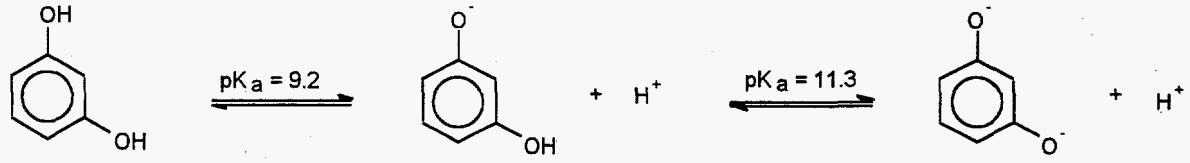

Figure 2-4. Acid/Base Equilibria of Diprotic Resorcinol

The effective capacities reported for R-F resin are 2.85 [4], 3.4 [5], and 6.35 meq/g [6]. The methods used to determine these capacities were different; Kurath et al. [5] suggest that a value around 3 meq/g is the correct effective capacity. The effective values of capacity are lower than the theoretical values possibly because many ion-exchange sites are converted into non-exchange sites as a result of oxidation and chemical reaction during synthesis and/or processing. Another possibility is that the three-dimensional structure of the resin may not allow presentation of many potential exchange sites. It is known that access to many sites is kinetically limited by particle diffusion [5]. For comparison, the theoretical capacity of the P-F resin, CS-100, is 9.4 meq/g. The manufacturer's listed capacity for this resin is >2 meq/g.

2.3 Selectivity of R-F Resin

The factors responsible for the observed selectivity of R-F resin are discussed qualitatively in this section, and consist of ion-exchange processes viewed from a thermodynamic or equilibria viewpoint. A discussion of the kinetics of ion-exchange for R-F resin may be found in Kurath et al. [5]. The information below is derived primarily from Helfferich [7].

Both R-F and P-F resins have similar polymer structures, which consist of highly crosslinked "islands" embedded in regions of low crosslinking. When the resin swells, regions of lower crosslinking expand while the highly crosslinked "islands" undergo little swelling. The density of highly crosslinked "islands" within a resin particle are very important in determining the selectivity characteristics of a resin, because it is in these regions that the size (which is related to solvation tendency) of the counter ion has the greatest effect on selectivity.

An important factor related to the selectivity of ion-exchange resins is the swelling characteristic of the resin. Swelling equilibrium is a balance of the opposing forces of the polar and ionic constituents of the resin to surround themselves with solvent and the elastic force of the polymer matrix to contract. The elastic force of the polymer matrix increases when the matrix is expanded and can be likened to a network of elastic springs which exert a pressure on the internal "pore" liquid. In thermodynamic

terms, the elasticity of the polymer matrix is due to an increase in entropy, which accompanies the coiling of the polymer chains. Entropy increases because a coiled configuration can be realized in a larger number of ways than a stretched one. The primary factors causing swelling of resins are as follows:

- The fixed and mobile ions of the resin are hydrated, i.e., they form solvation shells.
- The interior of the resin is a highly concentrated solution of ions, which tends to dilute itself by taking up more solvent, thus swelling the resin. This process can be viewed as an osmotic pressure difference between the interior of the resin and the external solution, and can also be expressed thermodynamically through the free energy of mixing. In the case of R-F resin, where there are areas of highly crosslinked polymer, the tendency of these areas to swell, as balanced by the contractive elastic force of the polymer matrix, gives rise to the high selectivity observed for cesium ion.
- Another force that expands the resin is that due to electrostatic interactions. Neighboring fixed ionic groups tend to repulse each other, thus swelling the polymer resin. In the case of R-F resin, the fixed ionic groups are the deprotonated hydroxyl groups on the resorcinol ring.

More specifically, the list of factors favoring swelling of resins are as follows:

- Polar solvents are better swelling agents because they interact more strongly with ions and polar functionalities within the resin. Commonly, the solvent used with organic ion-exchangers is water.
- The amount of crosslinking of the polymer resin plays an important role in resin swelling. Highly crosslinked resins don't swell as much as resins with lesser amounts (or regions) of crosslinking because the polymer network is simply more rigid. Expressed in terms of entropy, high crosslinking corresponds to a case where the polymer "chains" are shorter, hence expansion causes a greater loss in configurational entropy (swelling).
- The nature of the fixed ionic group and its affinity for polar solvents influences the amount of swelling observed for a resin. The greater the affinity for a polar solvent, the more strongly the resin swells. Resins swell to a greater extent when their ionogenic groups are completely ionized. For R-F resin, the resin swells more when the pH is 12 and above because, essentially, all the ring hydroxyl groups are deprotonated (they are in their ionic form).
- The capacity of the resin also plays an important role in the amount of swelling observed for a resin. A higher effective capacity corresponds to a greater number of ion-exchange sites. Swelling increases because there is a greater concentration of ions within the resin and the pore liquid has a greater tendency to dilute itself compared to a lower capacity resin. The effective capacity of R-F resin is slightly higher than the P-F resin, CS-100. The observed volume changes for R-F and CS-100 resins upon contact with NaOH are 43-54% and 22-28%, respectively [5].
- The effects on resin swelling produced by the counter ion is different for resins with differing amounts of crosslinking. For a moderate to highly crosslinked polymer resin, most of the solvent present is in the form of solvation shells about the fixed and mobile ions, and therefore the size and solvation tendency of the counter ion plays a crucial role in swelling and selectivity. The resin expands when a counter ion is replaced by another, which in its solvated state occupies a larger volume. For alkali ions, the sequence of increasing resin volume (swelling) is Cs < Rb < K <

Na < Li. This sequence is the same observed for the volume of the hydrated ions. For highly crosslinked resins, where solvation can be incomplete, this sequence can be partly reversed because the unsolvated lithium ion has a smaller volume than the unsolvated cesium ion. For weakly crosslinked resins, which contain large amounts of "free" solvent (as opposed to solvation shells), the valence of the ion is a more important factor in causing resin swelling. The tendency of the resin to take up free solvent depends on the number of counter ions in the resin. The amount of solvent taken up is halved when monovalent counterions are replaced by a divalent one, thus weakly crosslinked resins swell less when the valence of the counterion is high. As stated previously, R-F resin contains "islands" of high crosslinking embedded in lower crosslinking areas. This may help to explain the range of ion selectivities observed for R-F resin, which shows good selectivity for Cs^+ as well as Sr^{2+}, Cr^{6+}, Fe^{3+}, and Zr^{4+} [8]. The polyvalent ions may be more selectively retained in the areas of lower crosslinking, while the Cs^+ is selectively retained in higher-crosslinked portions of the resin.

- Swelling is reduced when counterions and fixed ionic groups associate or form complexes. This localization of counterions reduces the tendency to form solvation shells, thereby reducing the osmotic activity, thermodynamically, the free energy of mixing is reduced. For example, weak acid resins swell less when they are in the H^+ (or acid form) than when in an alkali-ion form.

- Resins that have been equilibrated with electrolyte solutions swell more strongly when the solution concentration of the electrolytes is low. This is rationalized again by the difference in osmotic pressure for the highly concentrated pore solutions of the resin compared to the dilute external solution.

Selectivity refers to the preferential retention of one counter-ionic species within the resin over another. The causes of selectivity are related to the valance of the counterion and the swelling of the resin as outlined above. Additional factors that may play a role in selectivity are sieve action and specific interactions within the resin and within the external solution. Sieve action is important for very large organic ions and inorganic complexes, and is essentially related to the steric requirements of the exchanging ionic species.

Many of the specific interactions within the resin have already been mentioned and are related to the tendency for counterions to associate or form complexes. For example, weak acid resins (such as P-F resins) have acid groups which tend not to dissociate completely. Predicted selectivities for these situations can be rationalized using Le Chatlier's Principle. Electrostatic effects are another interaction within the resin (there is higher selectivity for counterions of higher valance). The strength of electrostatic attraction of the mobile ion for the fixed ion is directly proportional to the ionic charge and inversely proportional to the square of the distance between charges. Hence, higher selectivity is generally observed for divalent ions over monovalent ions while the distance between the two attractive forces is also dependent upon the amount of solvation of the ionic species. A further factor within the resin affecting selectivity is the presence of London forces. London forces can be responsible for larger observed selectivities for ionic groups attached to nonpolar organic groups. Specific effects within the external solution are related again to factors such as counter-ion association with the co-ion (spectator ion). Here, the ion-exchanger prefers the counterion, which has a weaker association with the co-ion and can again be explained in terms of the Le Chatlier Principle.

For R-F resin, the primary cause of the observed selectivity of the resin for cesium in solutions with high sodium concentration is primarily related to the observed swelling of the resin. As shown in

Figure 2-5, swelling equilibrium is achieved by exchange of a sodium ion in the resin with a cesium ion from the external solution. When this exchange occurs, the resin is able to contract because the effective volume of the hydrated cesium ion is smaller than that of the hydrated sodium ion. This effect is most pronounced for resins or regions of resins where there is high strain or high crosslinking. Another factor related to the observed selectivity for cesium in high sodium concentration solution is the large Na^+/Cs^+ ion ratio, which favors higher selectivity because of the high swelling pressure of the R-F resin. One counteracting factor is the high ionic strength, for which the osmotic pressure within the resin is reduced. Solutions containing appreciable amounts of K+ and/or Rb+ ion can lower the selectivity of R-F resin for Cs^+ because these ions compete with Cs^+ for ion-exchange sites; R-F resin will selectively bind K^+ and Rb^+ in addition to Cs^+ relative to Na^+ over Na^+.

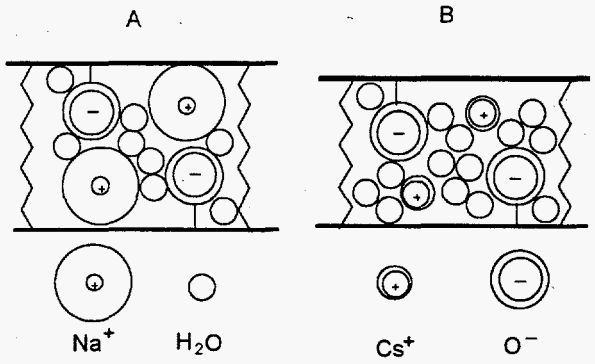

Figure 2-5. The Relationship Between (A) Swelling and (B) Contracting Due to the Selectivity Observed for Phenolic Condensation Polymers

3.0 Experimental

3.1 Preparation of Resins

The R-F resins used for this study were prepared at Boulder Scientific Co. (BSC) and at PNL. Resins from both sites were essentially prepared in identical fashion, except the batches from BSC were synthesized on industrial scale. The BSC resins studied consisted of two different batches stored in 55-gal containers and denoted as BSC-187 (manufactured 1988) and BSC-210 (manufactured 1993). R-F resins were typically prepared in 50-g batches at PNL. Duolite CS-100, a P-F resin, is manufactured by Rohm and Haas by special order in France and was obtained in 1991.

3.1.1 PNL-Synthesized R-F Resin

The synthesis of R-F resin was performed according to Wallace and Bibler's procedure [9], a variant of the procedure of Pennington and Williams [10], using the following modifications: (i) the preparation was halved; (ii) a pyrex baking dish (7" x 12") was used for curing the resin; (iii) a steady stream of air was introduced into the oven to aid in the removal of excess water from the oven chamber, and (iv) no activation of the resins was performed before characterization. A typical synthesis is described below: Resorcinol (33g, Aldrich, 99%) was dissolved in 250 mL of deionized water in a 500 mL beaker. A 6M KOH solution (16.8g KOH in 50 mL of deionized water) was added to the resorcinol solution with stirring. The initial color of the solution was a pale red-violet, which turned yellow brown within 1-2 min. The solution temperature was brought to 90 °C, stirred for 1 h, then cooled to room temperature. Formalin (87.5 mL, Aldrich, 37% solution) was added all at once to the resorcinol/KOH solution and stirred for 10 min. The whole mixture was poured into a pyrex baking dish (7" x 12") and placed in a conventional oven at 105 °C (the oven was situated in a fume hood) for about 20 h. The resulting hard glassy resin was then ground using a disk mill and sieved to obtain 20-50 mesh-sized particles. In general, all characterization of the resins was performed on the potassium salt form thus obtained; however some resins were converted to their acid forms as described below. Microanalyses for the PNL-synthesized resins, BSC-187, and BSC-210 were performed using a Perkin-Elmer Model 240-B Elemental Analyzer and/or by Schwartzkopf Analytical Laboratories.

3.1.2 Cesium Loading on R-F Resins, Varied Ionic Strength

The proton form of R-F resin BSC-210 was treated with cesium hydroxide in aqueous solution. Typically, the resin (2.5 g) was stirred with about 50 mL of aqueous CsOH under nitrogen. The CsOH solution contained varying amounts of cesium ion equivalent to 2.5%, 7.6%, 22.7%, 38.8%, 152.0%, and 609.8% of the theoretical number of exchange sites that would be contained in the resin sample. After contacting the resins with the CsOH solutions overnight, the samples were filtered and dried under vacuum, then analyzed using NMR and elemental analysis.

3.1.3 Cesium Loading on R-F Resins, Constant Ionic Strength

Solutions in which the Cs/Na ratio was varied were prepared by dissolution of the appropriate amount of CsOH and NaOH in water to make the 2.0M OH^- solutions with resulting Cs^+/Na^+ ratios of 1/99, 5/95, 15/85, 25/75, and 100/0. The solutions were stirred with about 3 g of BSC-210 (acid form) resin in 35 mL

of hydroxide solution under nitrogen. The samples were then filtered and dried under vacuum at 100 °C, then analyzed using NMR and elemental analysis.

3.1.4 Preparation of Acid Form of R-F Resins

The acid form of the resins were obtained by the following procedure: About 10 g of resin was stirred in a flask containing 150 mL of 1M formic acid under nitrogen for 70 h. The excess formic acid was filtered off the resin, and the procedure was repeated two more times with stirring for 2 h each time. The resins were filtered and rinsed with copious amounts of water, then air-dried for 2-3 days.

3.1.5 Oxidation of R-F Resins

Controlled air oxidation of CS-100 and R-F resins experiments were carried out using a high vacuum line outfitted with a gas uptake measurement apparatus. The polymer resins (typically 0.25 g) were dispersed in 50 mL 1M NaOH, 6 M NaOH, and Neutralized Current Acid Waste (NCAW) simulant supernate. The procedure consisted of sparging the NaOH or NCAW solutions with nitrogen, then the weighed-out resin sample was introduced into sparged solution and the vessel containing the resin and solution were placed on the gas uptake apparatus. The resin containing solution was then degassed using three freeze-pump-thaw cycles. After degassing and equilibration of the flask to atmospheric pressure with oxygen (the solution was not stirred until after equilibration), the uptake of oxygen by the resin was measured using the calibrated line. Related bulk air oxidation of the R-F resin (potassium form) was carried out by stirring 1 g of resin in a flask with 1M NaOH for 70 h, while sparging air through the solution. Oxidation of BSC-210 with oxygen was performed by a similar procedure involving 2.5 g of BSC-210 (acid form), 1M NaOH with varying amount of time so that the progession of resin oxidation/degradation could be monitored by ^{13}C solid-state NMR.

3.2 Distribution Coefficients, K_d's

The batch distribution coefficient ($K_d = [Cs]_{solid} \div [Cs]_{liquid}$) is an equilibrium measure of the overall ability of the solid phase ion exchange material to remove an ion from solution under the particular experimental conditions which exist after the contact. For the cesium K_d tests described in this report, 0.1 g of each "as received" material (normally the K^+-form) was placed into standard 20-mL scintillation vials and contacted with 15 mL of the 3.9M Na double-shell slurry feed (DSSF) simulant for 72 hours. The feed solution was "spiked" with approximately 12 nCi/mL ^{137}Cs and the cesium concentration was determined by gamma counting.[11]

The equation for calculating K_d (mL/g) can be simplified by measuring the analyte concentration before and after contact and calculating the quantity of analyte on the adsorbent by difference.

$$K_d = \frac{(C_i - C_f)}{C_f} * \frac{V}{M * F}$$

C_i is the initial concentration of the ion of interest in the feed solution prior to contact, C_f is the concentration after contact, V is the solution volume, M is the exchanger mass and F is the mass of dry ion exchanger divided by the mass of wet ion exchanger (F-factor). K_d (mL/g) represents the theoretical

volume of solution that can be processed per mass of exchanger under equilibrium conditions. The F-factor was determined by drying the material at 105°C for 24 hours.

Table 3.1. DSSF Simulant Composition

Species	DSSF, M
Na^+	3.90 E+00
K^+	9.23 E-02
Rb^+	8.57 E-05
Cs^+	7.00 E-05
Sr^{2+}	6.00 E-07
Al^{3+}	3.43 E-01
SO_4^{2-}	1.19 E-01
HPO_4^{2-}	1.98 E-02
OH^- (free)	1.32 E+00
OH^- (total)	4.08 E+00
CO_3^{2-}	1.58 E-01
NO_2^-	3.43 E-01
NO_3^-	1.32 E+00
F^-	7.05 E-02

3.3 Nuclear Magnetic Resonance Spectroscopy

Solid-state NMR spectra were obtained with a Varian Associates model VXR-300 spectrometer system equipped with ultra high-speed cross polarization/magic angle spinning (CP-MAS) solid-state probes (Doty Scientific, Inc.), and with a Chemagnetics model CMX-300/100 solid-state NMR spectrometer equipped with Chemagnetics high-speed spinning CP-MAS probes.

CP-MAS spectra were obtained using 4.5 μs 90° proton pulses, 2 ms contact times, and about 55 kHz high power decoupling amplitudes with two-second recycle delays. Spectra were collected at 12 kHz magic angle spinning speeds, necessitating an offset of the carbon matching amplitude by 12 kHz from the static Hartman-Hahn match.

Single pulse excitation (Bloch decay) spectra were obtained using a 4.5 μs 90° carbon observe pulse with 55 kHz proton dipolar-decoupling during carbon free induction decay (FID) acquisition.

3.4 Fourier Transform Infrared Spectroscopy

Fourier Transform Infrared (FTIR) spectra were obtained using a Nicolet Model 740 FTIR spectrometer outfitted with deuterium triglycine sulfate (DTGS) detector. Typically, resin samples of 100-200 mesh were ground with KBr for 30 s and then pressed into pellets. The spectra obtained in this fashion were representative of the bulk samples.

In addition, surface reflectance spectra were obtained by use of a Nic-Plan IR Microscope attached to the Nicolet FTIR spectrometer. The spectra obtained by use of the IR microscope were indicative of the IR absorbances on the surface of the resin.

3.5 Thermogravimetric/Infrared Analysis, Brunauer, Emmett, Teller Surface Area/Pore Structure Analysis, Scanning Electron Microscopy, and X-Ray Diffraction

TGA/IR analysis of R-F resin 55197-2-A was performed at PNL using a Perkin Elmer Model TGA7 analyzer interfaced with a Nicolet 800 FTIR spectrometer. The composition of the gases evolved in the TGA was monitored continuously using FTIR. The TGA was temperature-calibrated using the curie point transition temperatures of Alumel and Perkalloy and weight-calibrated using a Class S 100 mg weight. The purge gas used throughout the TGA and FTIR instrument was argon. The IR spectrum of the purge gas was monitored for 10 minutes to obtain a background and reference spectrum. The system was then purged for 14 min to remove air after introduction of the resin into the sample chamber to remove IR active gases from the system before heating the sample. BET surface area/pore structure analysis was performed according to literature methods [12].

3.6 Radiolytic Stability of R-F and CS-100 Resins

To determine the effect of gamma radiation on R-F resins BSC-187 and BSC-210, and CS-100 resin, cesium distribution values were determined for untreated resin (no gamma) and resin that had been irradiated for various intervals up to ~10E9 Rad. The resin was tested in two ways, under flowing conditions or in a static solution. In each case, the solution used was synthetic NCAW. The tests were designed to determine differences between the flowing and static systems, and to determine the stability of R-F resin as a function of dose.

The R-F and CS-100 resins were irradiated within NCAW simulated waste supernate under flow (NCAW flow at 0.5 CV/h) and static conditions at 2×10^5 R/h for up to 4000 h gamma exposure (^{60}Co gamma source) for a total of approximately 1×10^9 R. To determine the gas generation for the supernate solution in the absence of resin, NCAW-simulated waste supernate was irradiated under static conditions at a dose rate of 1.5×10^5 R/h (^{60}Co gamma source) for a total of 2270 h for a total dose of 2.4×10^8 R.

4.0 Evaluation of CS-100 and R-F Ion Exchange Resins

This section provides a structure/function analysis of the PNL-synthesized R-F resins, BSC-187 and BSC-210, as well as some experimental data for CS-100 resin. The first section describes the experimentally determined cesium selective K_d, which are an indicator of resin performance. Subsequent sections present the details of the structural characterization of R-F resin, with special emphasis placed on NMR and IR techniques, and includes an examination of the structure/ function relationship for cesium-loaded R-F resin. The final two sections describe analysis of the chemical and radiolytic stability of R-F and CS-100 resins.

4.1 Distribution Coefficients

The primary indicator used to evaluate the selectivity performance of an ion-exchange resin is the K_d. The idealized equilibrium process, which occurs for a Na^+/Cs^+ ion exchange, is represented in Eq. [1], where Cs^+ and Na^+ are ions in the external solution while NaS and CsS represent these counterions attached to anionic sites (with site concentration S) within the exchanger.

$$Cs^+ + NaS \rightleftharpoons Na^+ + CsS \qquad [1]$$

The ion-exchange equilibrium constant for the above reaction is given in Eq.[2]:

$$K_{eq} = [CsS][Na^+]/[NaS][Cs^+] \qquad [2]$$

The units for [Na+] and [Cs+] are moles/L or meq/mL while the units for [CsS] and [NaS] are meq/g. The ion exchange process represented in Eq. [1] is given in Eq. [3]. It can be seen that the units of the K_d are mL/g and that K_d represents half the total equilibrium constant expression, Eq. [2], so K_d should not be treated as an equilibrium constant. However, if K_{eq} is known, K_d can always be calculated.

$$K_d = [CsS]/[Cs^+] \qquad [3]$$

The above equations are representative of an idealized ion-exchange process that assumes the following: only one type of site is present in the exchanger; the site is insensitive to solution conditions; ion concentrations can be used instead of ion activities; the structure of the exchanger is invariant (no swelling or contraction); and only the two ions, Cs^+ and Na^+, are competing for the site[13]. These conditions rarely exist in reality; however, the above description provides a useful basis for understanding the meaning of K_d.

Most resins studied have been evaluated for K_d's using resins containing K^+, which may compete with Cs^+ for exchange sites. Therefore, the K_d's must be understood within the context of each individual sample. The K_d evaluations of the PNL-synthesized resins have been performed using the K^+ form so that comparison of K_d's for BSC samples and PNL samples were made on a uniform basis. Although the rigorous approach would be to convert all resins to their acid forms for evaluation, the indications are that oxidation of the resins may occur during certain acid workup conditions, so the K^+ form of the resins were used as the basis for standard evaluation.

Table 4-1 lists the K_d's for R-F and derivative R-F resins prepared at PNL and at BSC. Samples were run in duplicate. BSC-187 was run several times and effectively served as a control for the determinations carried out on the PNL-synthesized resins. The K_d values obtained for the BSC-187 resin were consistently of smaller magnitude than the R-F resin prepared at PNL, which is probably subject to oxidation/ degradation with time as a combined result of the age of the resin (prepared in 1988) and a non-optimized synthetic procedure. The BSC-210 batch of resin prepared in 1993 gave K_d's that were similar to those of the PNL R-F resins (samples 54677-120-A, 54677-128-A, 55197-1-A, 55197-2-A, and 55197-2-B), although the PNL R-F resins had K_d's that were an average of 14% higher. Some of the initial preparations of R-F resin at PNL had very low K_d's because the resin was not cured properly during synthesis (i.e., samples 54677-118-A, 54677-118-B, and 54677-121-A).

Table 4-1. Distribution Coefficients for Resorcinol-Formaldehyde Ion-Exchange Resins

Sample		K_d	Comments
PNL	54677-118-A	559, 632	H_2O washed; insuff. curing
PNL	54677-118-B	453, 460	Insufficient curing
PNL	54677-121-A	65, 70	118-A washed w/ 2M NaOH
PNL	54677-120-A	4113, 4223	Anaerobic synthesis
PNL	54677-128-A	4875, 5192	Standard synthesis
PNL	55197-1-A	5961, 6345	^{13}C-labeled formaldehyde
PNL	55197-2-A	5909, 5557	Standard synthesis
PNL	55197-2-B	5522, 5794	^{13}C-labeled methanol
PNL	55197-15-A	2365, 2481	25 °C cure(2 wks), then 105°C
PNL	55197-15-B	1244, 1183	15-A cured in *n*-butanol
PNL	55197-16-A	3, 4	Glyoxal, 100%
PNL	55197-35-A	6, 3	Glyoxal, 100%
PNL	55197-36-A	2549, 2499	Glyoxal, 5%
PNL	55197-38-A	3230, 3377	Octane reflux reaction mixture
PNL	55197-38-B	2995, 3138	Cured at 216 °C
PNL	55197-41-A	4396, 4722	LiOH base instead of KOH
PNL	55197-42-A	1748, 1822	K_2CO_3 base instead of KOH
PNL	55197-55-A	84, 90	Terepthaldialdehyde, 100%
PNL	55197-56-A	1439, 1692	Terepthaldialdehyde, 15%
PNL	55197-58-A	2055, 1944	Phloroglucinol, 10%
PNL	55197-59-A	75, 76	Phloroglucinol, 100%
BSC	BSC187	3444, 3420	
BSC	BSC187	3530, 3436	
BSC	BSC187	3958, 4058	
BSC	BSC187	3534, 3378	
BSC	BSC187	3502, 3328	
BSC	BSC187	3489, 3530	
BSC	BSC187	3489, 3530	
BSC	BSC210	4655, 4580	

Resin 54677-120-A was prepared under anaerobic conditions to examine the effect that exclusion of air would have on the performance of the resin. Resin degradation is thought to occur because of air oxidation. The average K_d for this resin was 4168 mL/g, a value slightly lower than resins prepared under standard atmospheric conditions. The most likely reason for the slightly lower K_d value is that the resin was not as efficiently cured, hence crosslinked, as resin prepared under standard atmospheric conditions in an oven. Preparation under anaerobic conditions was carried out in a resin kettle under a nitrogen atmosphere, and elimination of water was not as efficient. This synthetic procedure has not yet been optimized, however. The ^{13}C-labeled resin 55197-1-A, prepared by enriching formaldehyde with $H^{13}C(O)H$, gave the largest K_d observed for the PNL resins, although exact reason(s) for this observation are unknown. Another resin was prepared with excess $H_3{}^{13}COH$ to determine if methanol from the formalin solution was being incorporated into the resin. The NMR studies (*vide infra*) indicate that the methanol in the formalin solution is not incorporated into the R-F resin and most of the methanol is evaporated during resin curing. Resin 55197-15-A was prepared using a standard R-F precursor solution (30 mL) and was cured for two weeks at room temperature in an open beaker, then the resin disk was transferred to the oven for final curing (20 h at 105 °C). The distribution coefficients for this resin were well below those prepared under standard conditions, probably because there was insufficient crosslinking of the polymer resin as a result of the lower temperature. A 10 mL portion of resin 55197-15-A precursor solution was placed in a vial containing about 20 mL of *n*-butanol and cured (same conditions as resin 55197-15-A) to give resin 55197-15-B. Curing in the butanol lowered the distribution coefficients.

It was assumed that increasing the surface area of the resin would enhance the performance of the resin by providing access to more ion-exchange sites. In an attempt to prepare macroreticular resins, which have large fixed pores and thus much greater surface area, different crosslinking agents were used. For example, glyoxal and terepthaldicarboxaldehyde condensations with resorcinol were attempted. The idea was that these materials would provide a resin structure with large fixed pores, similar to styrene-divinylbenzene resins. R-F resin, in which 100% of the crosslinker was glyoxal, gave essentially no cesium ion-exchange. The "resin" that resulted from this reaction was very soft and easily ground to a fine powder using a mortar and pestle. Resin 55197-36-A prepared by crosslinking resorcinol with a mixture of 95% formaldehyde and 5% glyoxal essentially halved the K_d value expected for a typical R-F resin. Similarly, Resin 55197-55-A, prepared from resorcinol with 100% terepthaldicarboxaldehyde as crosslinker, gave essentially no cesium ion-exchange while the R-F resin 55197-56-A, prepared using 85% formaldehyde and 15% terepthaldicarboxaldehyde as the crosslinking units, gave K_d's about one fourth of the standard R-F resin. One other attempt to create pore structure in the R-F resin was carried out by substituting K_2CO_3 for KOH in the reaction. The idea was that during curing and or conversion to the acid resin form, CO_2 gas could be eliminated from the gel resin, thus creating pore structure. The reaction took a very different course, however. Upon addition of the formalin solution to the resorcinol solution, the reaction mixture immediately gelled. The gelatinous material was placed in the oven and cured as usual, and the resin thus obtained had a fairly typical appearance. However, the Kd's for this resin were about one-third that observed for standard R-F resin. Apparently, use of this base does not allow the condensation at the resorcinol ring to proceed as extensively, and indeed this is part of the approach used to make low-density carbon aerogels [14].

Another resin variation that was examined was 10% and 100% phloroglucinol (1,3,5-trihydroxybenzene) containing resins. For phloroglucinol, all of the ring condensation sites are equivalent, and theoretically, the capacity of resins containing phloroglucinol should be increased. However, these resins showed poor cesium selectivity and NMR spectra showed that these resins contained very large amounts of ketones and quinones, which indicated significant oxidation of the resin.

One batch of R-F resin (55197-41-A) was prepared using LiOH in place of KOH. The reason for using KOH, as set forth in Bibler's patent [9], is that there is a templating effect during the curing of the resin, such that the correct pore and cavity size are created in the resin matrix, which enhances the selectivity of the resin for cesium ion. The high Kd's obtained for the LiOH preparation of R-F resin casts some doubt on this theory because the effective size of the lithium cation is significantly larger than the potassium cation, therefore the selectivity should be altered.

The effect of curing temperature on the quality of the resins was examined for the temperature range of 105-400 °C. Samples of resin 55197-2-B were placed in a small tube furnace under an atmosphere of helium for curing at temperatures above 105 °C. The results are given in Table 4-2. The distribution coefficients showed a steady decrease in the selectivity of the resin. The reason for the decrease in ion-exchange capacity is unclear, however, chemical decomposition (hence deactivation) of ion-exchange sites seems likely.

Table 4-2. Effect of Temperature on Distribution Coefficients for Resin 55197-2-B

Sample		K_d	Comments
PNL	55197-2-B	5522, 5794	standard 105 °C curing
PNL	4252-60-A	4438, 4304	curing at 200 °C
PNL	4252-60-B	1236, 1135	curing at 300 °C
PNL	4252-60-C	49, 47	curing at 400 °C

The results presented in Table 4-3 for PNL resin 55197-15-C suggests that 20-50 mesh size particles are the optimal size for desirable ion-exchange characteristics. The smaller distribution coefficients obtained for the larger particles is observed because ion-exchange is particle diffusion limited. The results observed for the smaller particles may result from polymer breakdown/oxidation during the mechanical grinding process or possibly because the surface sites have lower selectivity than the interior sites. The ratio of surface to internal sites is increased for the smaller size particles.

Table 4-3. Effect of Particle Size on Distribution Coefficients for Resin 55197-15-C

Sample		K_d	Comments
PNL	55197-15-C	3945, 4051	particles >20 mesh
PNL	55197-15-C	5467, 5276	particles 20-50 mesh
PNL	55197-15-C	4472, 4466	particles <50 mesh
PNL	55197-15-C	2642, 2550	very fine particles

4.2 Structural Characterization

The primary methods used to structurally characterize the resins were ^{13}C CP-MAS solid-state NMR and FTIR spectroscopy. Additional characterization methods such as elemental analysis, TGA, SEM, and BET surface area/pore structure analysis were also used to derive basic information about the R-F resins. These studies have led to the conclusion that the primary polymer unit of the R-F resin consists of a 1,2,3,4-tetrasubstituted resorcinol ring, with the methylene linkages occurring at the 2 and 4 positions of the ring (see Figure 2-3).

4.2.1 NMR Spectral Characterization of R-F Resin

To establish the approximate expected chemical shifts for the carbon NMR spectrum of R-F resin, the baseline ^{13}C NMR spectrum of resorcinol (solution, D_2O) was obtained and gave the following resonances and carbon atom assignments (refer to Figure 2-3): 155.9 ppm (C-1, C-3, *ipso*); 130.8 ppm (C-5); 107.6 ppm (C4-C-6); 102.6 ppm (C-2). Solid-state ^{13}C CP-MAS NMR of neat resorcinol gave the same spectrum; however, acquisition of the spectra required longer relaxation times than usual so that the carbon signals could be observed.

The solid-state ^{13}C CP-MAS NMR spectra of a cyclic oligomer of resorcinol, *C*-undecylcalix-[4]-resorcinarene (Figure 4.1) [15] was also recorded for comparative purposes. The solid-state spectrum parallels the solution spectrum, and the resonance frequencies and assignments for the aromatic carbons are 150.6 ppm, 150.3 ppm (C-1, C-3 *ipso*); 124.9 ppm (C-2, C-6); 123.9 ppm (C-5); 102.5 ppm (C-5). This spectrum is important in that it shows excellent resolution of the two *ipso* carbons which are inequivalent due to tautomerization (hydrogen-bonded ring hydroxyl tautomers are "frozen" in the solid state) and gives the approximate NMR frequencies for the aromatic carbons of a 1,2,4,5-tetrasubstituted resorcinol ring unit. Calculation of chemical shifts[a] for model compounds (Figure 4.2) of 1,2,4,5- and 1,2,3,4-tetrasubstituted resorcinol rings gave the following chemical shifts: (A) 156.1 ppm (C-1, C-3); 131.1 ppm (C-5);

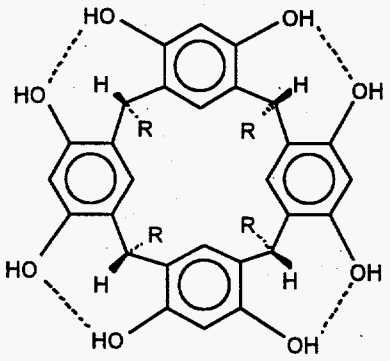

Figure 4.1. *C*-undecylcalix-[4]-resorcinarene (R = undecyl)

[a] The chemical shifts were calculated using the ^{13}C NMR Module software installed on ChemWindow, v. 3.0, Softshell International, Grand Junction, Colorado.

Figure 4.2. Model Structures Used to Calculate ^{13}C NMR Chemicals Shifts for A) 1,2,4,5- and B)1,2,3,4-tetrasubstituted Resorcinol Rings

123.3 ppm (C-4, C-6); 103.9 ppm (C-2). (B) 158.5 ppm (C-3); 156.1 ppm (C-1); 128.7 ppm (C-5); 123.3 ppm (C-4); 117.9 ppm (C-2); 109.3 ppm (C-6). These calculations suggest that the high field resonance observable for a 1,2,4,5-tetrasubstituted ring system (A) should occur at about 104 ppm, while a 1,2,3,4-tetrasubstituted ring system as in B should have resonances at chemical shifts no lower than 109 ppm. For spectra of R-F resin (Figure 4.3), there is little if any absorption of radiation observed in the 100-110 ppm region, and the spectra actually obtained are consistent with the 1,2,3,4-tetrasubstituted ring structure.

Examination of the spectra for the R-F resin (Figure 4.3) shows that there are three main resonance frequency domains. All R-F resin spectra were obtained using the mono-potassium salt form unless otherwise noted. Resonance at 152.4 ppm is assigned to the ring *ipso*-OH carbons, while the most intense resonance occurring at 120.9 ppm results from the balance of the ring carbons. The third main domain is assigned to the bridging methylene carbons in the polymer resin with a frequency range of 26-35 ppm. A closer look at each domain reveals a few more details. For both resonances at 152 ppm and 120 ppm there are shoulders on the low field side of each resonance (frequencies are about 158 ppm and 130 ppm, respectively). The methylene resonance at 26 ppm is preceded by two less intense but distinct resonances at 10 ppm and 16 ppm. Comparison of the resin spectra to the spectra for *C*-undecylcalix-[4]-resorcinarene (Figure 4.4) indicates that the resorcinol ring in the resin has a different substitution pattern than that observed for the calixarene because of the absence of resonance around 103 ppm.

Preparation of ^{13}C-labeled resins using $H^*C(O)H$ and $^*CH_3OH$ (Cambridge Isotope Laboratories, 99%) was performed to selectively enhance NMR signals in the resins. Resin 55197-1-A was synthesized by enriching the formalin solution with ^{13}C-labeled formaldehyde. The solid-state ^{13}C NMR (Figure 4.5) showed that there was some residual formaldehyde in the polymer resin with the appearance of a sharp resonance at 171.3 ppm. As expected, the methylene carbon resonances were greatly enhanced and partial resolution into two peaks roughly of equal intensity was observed (30.1 ppm and 26.6 ppm). Additionally, sharp resonances were observed at 16.7 ppm and 10.5 ppm. These results are consistent with condensation of the formaldehyde to form methyl groups at the C-2 and C-4 positions of the resorcinol ring. The partial resolution of the methylene resonance into two peaks indicates that there are two nonequivalent bridging methylene groups. There are two possible ring substitution patterns that will give rise to two non-equivalent methylene signals: 1,2,3,4-tetrasubstitution, and 1,2,3,5-tetrasubstitution.

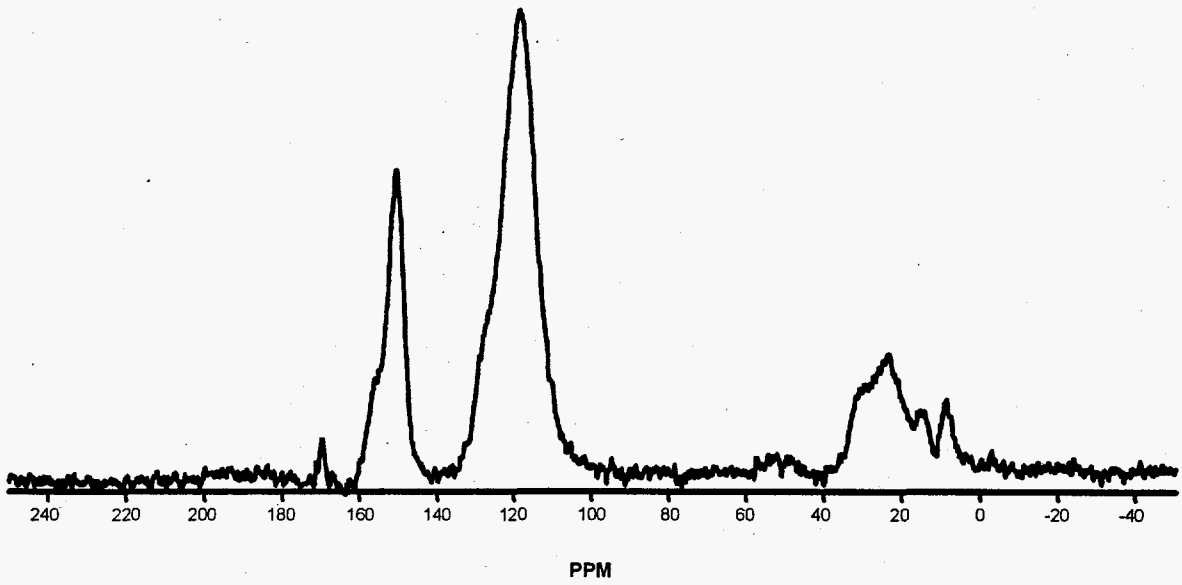

Figure 4-3. ^{13}C NMR of Resorcinol-Formaldehyde Resin (2-A)

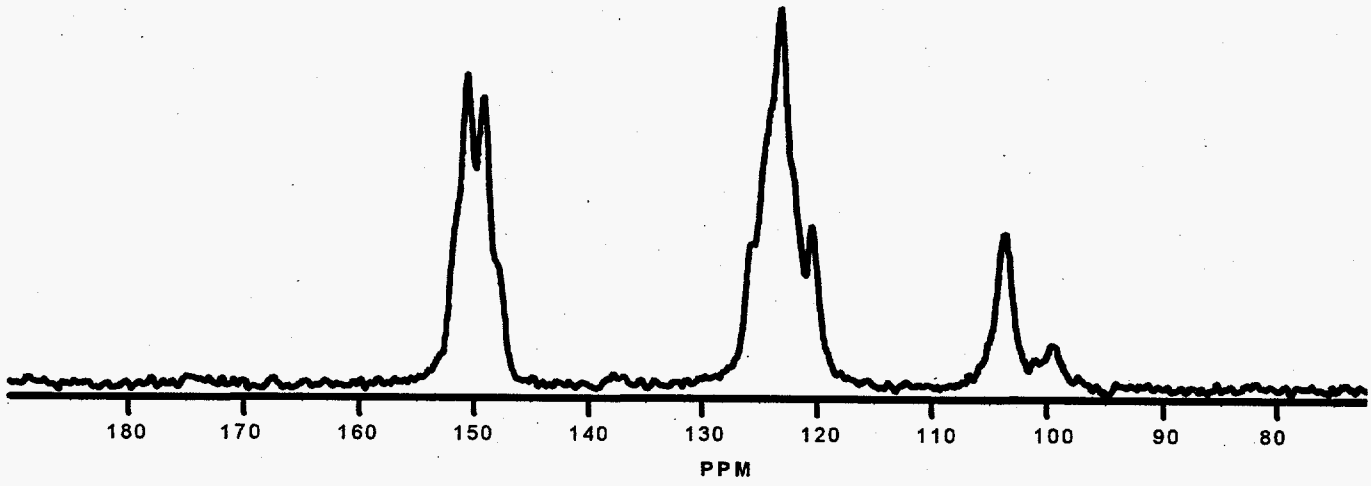

Figure 4-4. ^{13}C NMR of C-Undecylcalix-[4]-resorcinarene

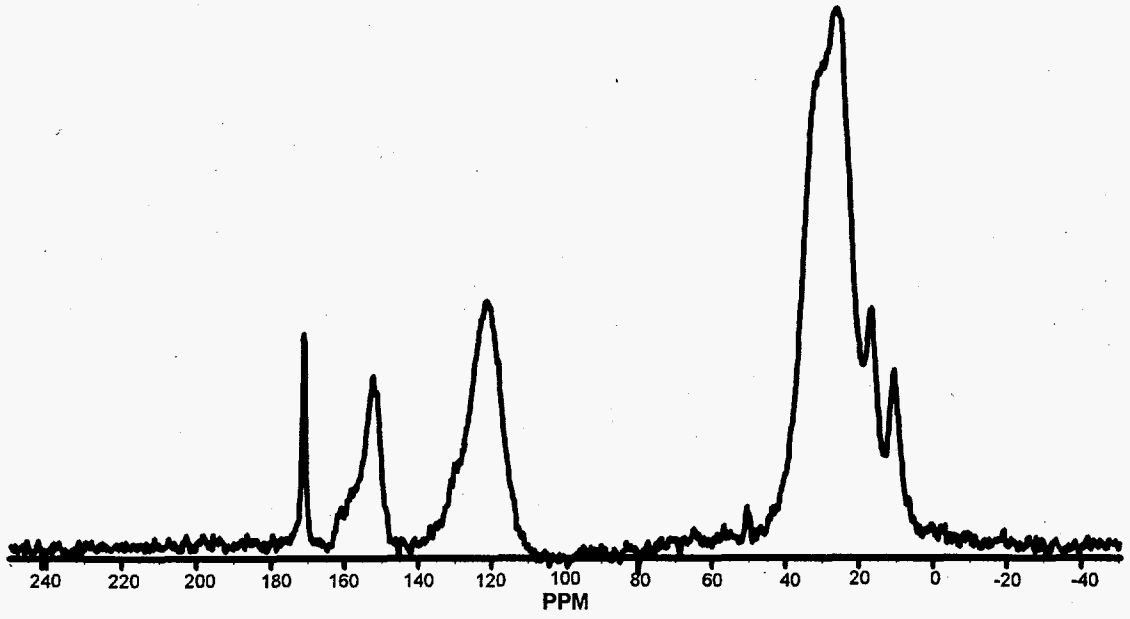

Figure 4-5. ^{13}C NMR of R-F Resin Prepared with ^{13}C-Labeled Formaldehyde

The C-5 position, which is *meta* to both hydroxyl groups, is deactivated towards substitution, thus only the 1,2,3,4- ring substitution (Figure 4-2B) pattern occurs for which there are two possible pathways to arrive at this pattern (condensation at C-2 and C-4 *or* C-2 and C-6). Similar structures for R-F oligomers have been observed using solution NMR studies [16].

A resin was prepared that incorporated ^{13}C-labeled methanol in an attempt to determine the synthetic consequences arising from the presence of methanol during resin synthesis. Standard formalin solutions used to prepare resins are aqueous solutions of 37% formaldehyde and 15% methanol (the methanol serves as a polymerization inhibitor for the formaldehyde). Resin 55197-2-B was enriched with ^{13}C-labeled methanol and its ^{13}C NMR (Figure 4.6) showed that there is residual methanol trapped in the polymeric resin by a sharp resonance at 49.9 ppm. Additional resonances occurred from 53.2 ppm to 58.1 ppm indicating the presence of methoxy and/or $-CH_2OCH_2-$ groups[17]. It is difficult to determine if the methoxy/ether groups are chemically bound to the polymer or if these methoxy groups are present as the acetal or hemi-acetal form of the formaldehyde either as a monomer or oligomer within the resin matrix.

One of the goals of the NMR studies was to gather baseline spectroscopic data for R-F resin in its different ionic forms to discern any structural changes that may accompany the ion-exchange process. Figure 4.7 compares the ^{13}C CP-MAS NMR spectra of BSC-210 R-F resin in different ionic forms. The first spectrum is of the standard potassium "as prepared" form, while the subsequent spectra show the resulting changes that occur after contacting BSC-187 resin with 2M CsOH, 2M NaOH, 6M NaOH, and 1M formic acid. The spectra are essentially identical for the potassium, sodium, and cesium ionic forms of the resin. However, when the resin has been contacted with the 6M NaOH solution, a downfield shift to about 165 ppm occurs for the ring hydroxyl carbon resonance. At higher ion-loading, ionization of both

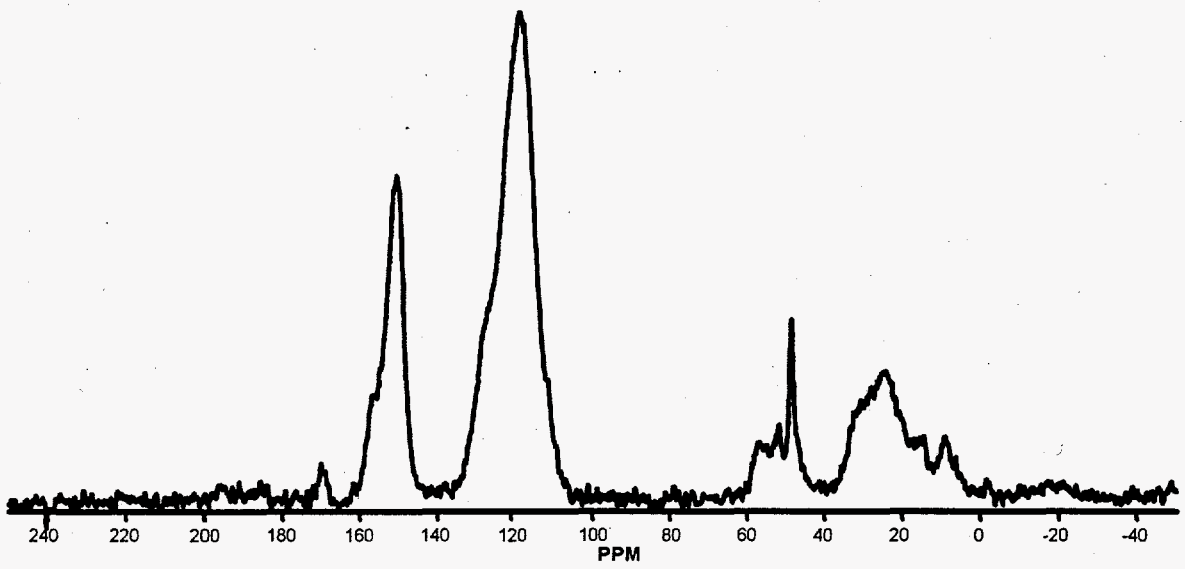

Figure 4.6. ^{13}C NMR Spectra of R-F Resin Prepared with ^{13}C-Labeled Methanol

hydroxyl groups on each ring is expected to occur and the 165 ppm resonance may be indicative of resin, which has high ion-loading and suggests that NMR can be used to monitor the amount of ion-loading occurring for a particular resin sample. The spectrum of the resin treated with 1M formic acid shows a fairly sharp resonance for the ring hydroxyl carbons at 151 ppm and partial resolution of the remainder of the aromatic carbons with resonances at about 131 and 120 ppm. The difference between spectra for ionic and acid forms of the R-F resin suggests that NMR may be used to monitor resin product quality.

In summary, the ^{13}C NMR spectra show that the main pattern of substitution for a resorcinol ring unit of the polymer resin is 1,2,3,4-tetrasubstituted, and that small amounts of formaldehyde and methanol are trapped in the polymer matrix. Resins exhibiting poor cesium uptake characteristics exhibit very broad resonances suggestive that oxidation of the resin to give quinoid ring structures has taken place.

4.2.2 Infrared Characterization of R-F Resin

The infrared spectrum of resorcinol (Figure 4-8) and C-undecylcalix-[4]-resorcinarene (Figure 4-9) have been examined to provide a baseline comparison for the IR spectra of the resins. Samples were prepared as KBr pellets. All assignments are based upon known group frequencies for organic molecules.

The IR spectrum for resorcinol (Figure 4-8) shows a very intense broad band at 3255 cm^{-1}, ν(O-H), for the hydroxyl groups on the ring and the intensity and frequency are indicative of strong intermolecular hydrogen bonding. The presence of water also contributes to this band. Other diagnostic bands corresponding to ν(C=C) "skeletal ring vibrations," ν(C-O), and δ(C-H) aromatic out of plane bending vibrations occur in the 2000 to 400 cm^{-1} frequency range. The aromatic δ(C-H) bending vibrations (773 and 740 cm^{-1}) are especially important because they give information about the ring substitution pattern. The weak bands between 2000 to 1660 cm^{-1} are overtone bands, which give information about the ring substitution pattern as well. The major bands and their assignments are given in Table 4-4.

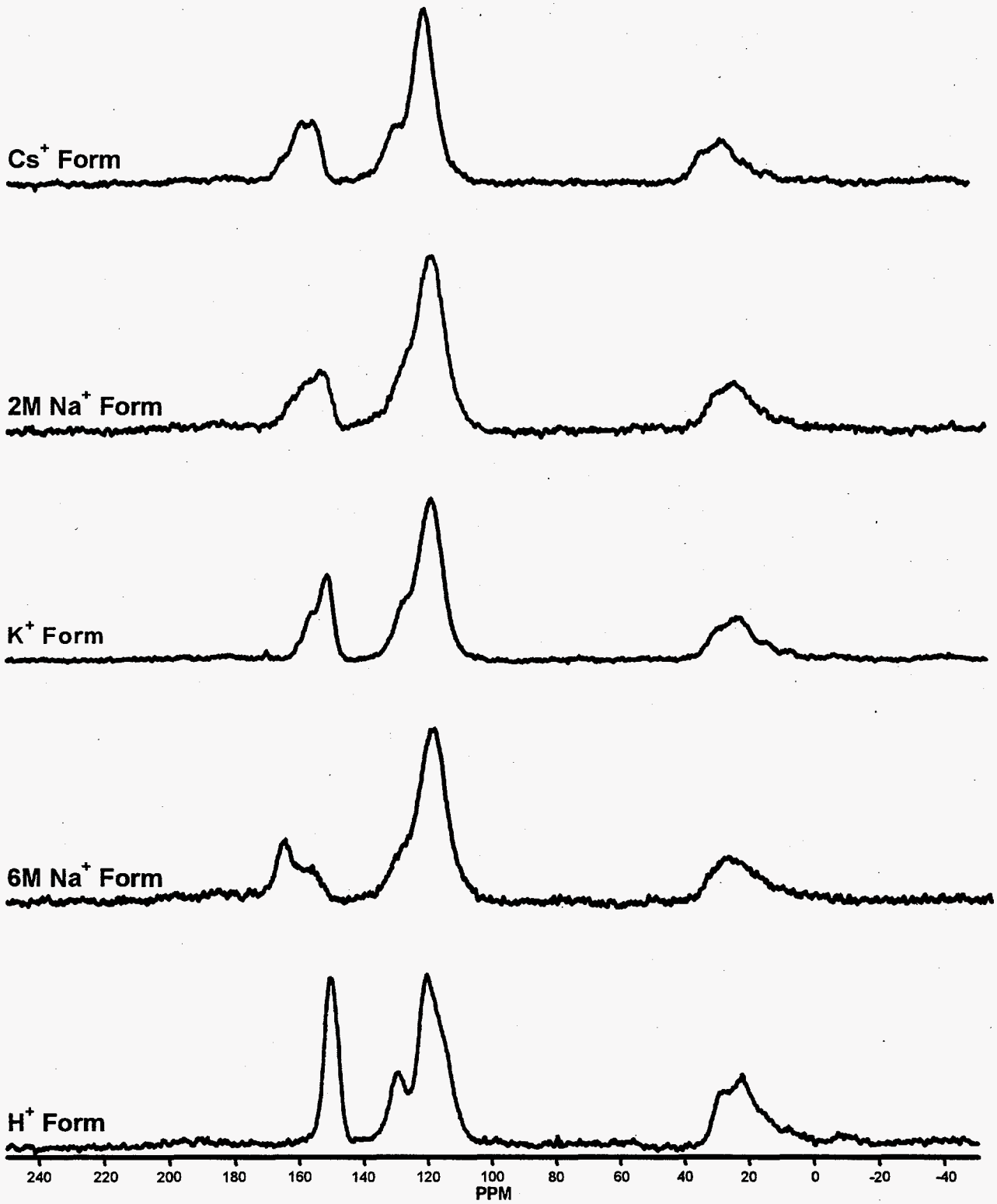

Figure 4-7. ^{13}C NMR of BSC-210 in Different Ionic Forms

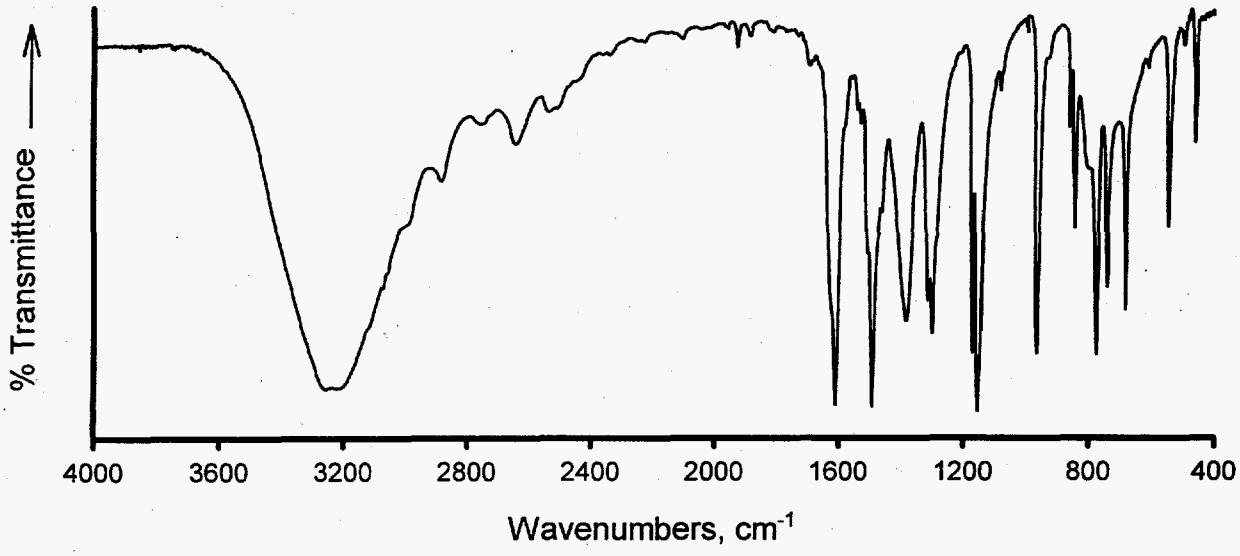

Figure 4-8. Infrared Spectrum for Resorcinol, KBr Pellet

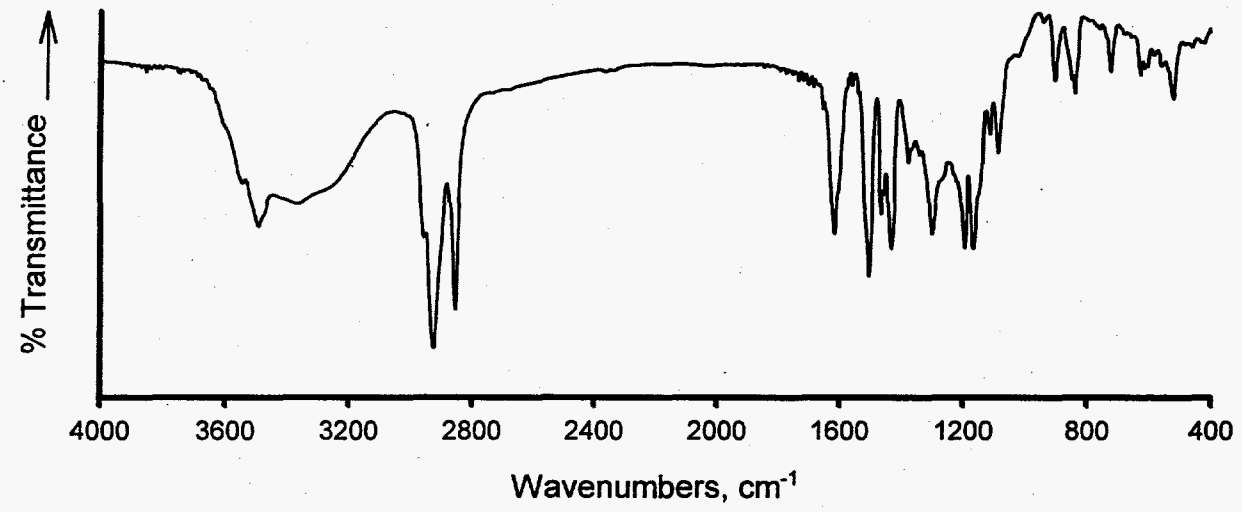

Figure 4-9. Infrared Spectrum for C-Undecylcalix[4]resorcinarene Monohydrate, KBr Pellet

Table 4-4. Bands and Assignments for the IR Spectrum of Resorcinol

Band, (cm^{-1})	Assignment
3255	ν(O-H) intermolecular H-bonding
1608 w/ sh 1490 w/ sh	ν(C=C) "ring breathing"
1380, 1311, 1297	δ(O-H) in plane bending
1167, 1152	ν(C-O) symmetric and asymmetric stretching
773, 740	δ(C-H) aromatic out of plane bending indicative of 1,3-disubstitution
680	δ(C-C) out of plane ring bend

The IR spectrum of *C*-undecyl-[4]-calixresorcinarene (Figure 4-9) provided some useful structural comparison data about the substitution pattern of the resorcinol ring. The primary band of importance for this spectrum was the aromatic C-H deformation band observed at 836 cm^{-1}, which is structural indication of a 1,2,4,5-tetrasubstituted resorcinol ring and is consistent with the NMR data previously discussed. The ν(C-O) vibrations occur at 1195 and 1168 cm^{-1} while the ring skeletal vibrations, ν(C=C), are observed at 1616 and 1505 cm^{-1}. All bands are shifted to a higher frequency compared to resorcinol.

The IR spectrum of R-F resin 55197-1-A (Figure 4-10) is representative of IR spectra of R-F resin in general. The broad band at 3436 cm^{-1} is indicative of O-H bond stretching from the ring hydroxyls and water. The strong band at 2964 cm^{-1} and the small companion band at 2908 cm^{-1} arise from the C-H stretching of the methylene linkages and occur at higher frequencies because of the rigid polymer framework. The ring skeletal vibrations appear as medium weak bands at 1633 and 1414 cm^{-1}. The strong sharp band at 1260 cm^{-1} is likely a coupled vibration between the ν(C-O) and ν(O-H). The two very strong bands at 1097 and 1027 cm^{-1} are assigned as C-O stretching bands, representing symmetric and asymmetric C-O stretching. The other very strong band at 802 cm^{-1} is the aromatic C-H out-of-plane deformation band and indicates that the ring substitution pattern is 1,2,3,4-tetrasubstituted. The small shoulder band at 865 cm^{-1} is another aromatic δ(C-H) band which may indicate either 1,2,4,5-tetrasubstitution, pentasubstitution, or 1,2,4-trisubstitution of the ring units. A qualitative comparison of the bands suggest that the 1,2,3,4-tetrasubstituted ring structure compromises 85-90% of the polymer resin. The bands and assignments are listed in Table 4-5.

Infrared spectra in conjunction with the NMR data indicate that the major condensation sites on the resorcinol ring occur at C-2, C-4, and C-6 to give 1,2,3,4-tetrasubstituted rings as the primary unit of the polymer resins. The polymer resin may also contain 1,2,4-trisubstituted, 1,2,4,5-tetrasubstituted, and pentasubstituted ring units from the condensation reaction, which make up 15% or less of the resin. Using

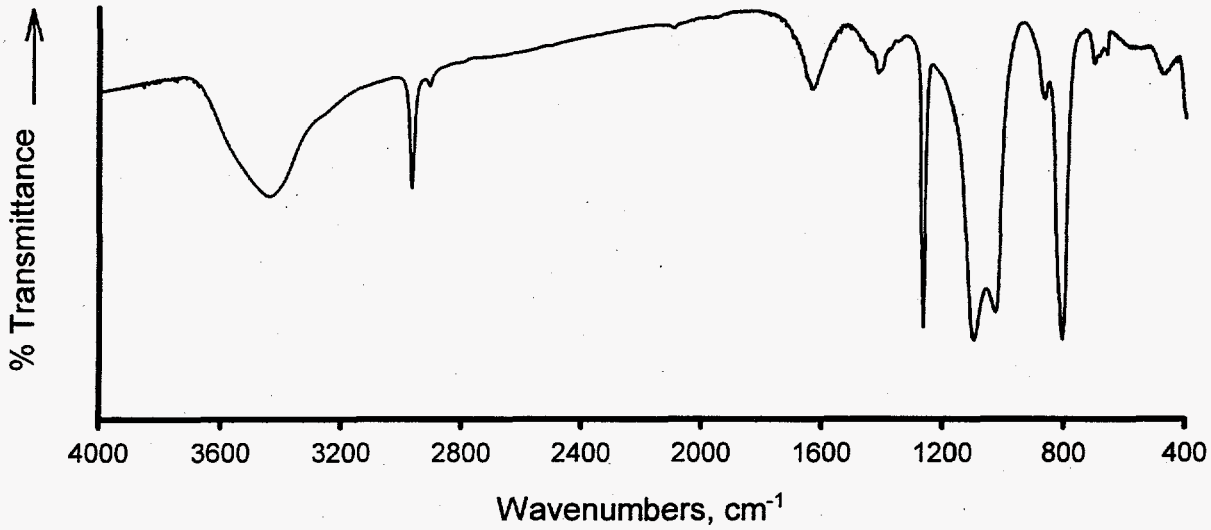

Figure 4-10. Infrared Spectrum of R-F Resin 55197-1-A, KBr Pellet

Table 4-5. Bands and Assignments for the IR Spectrum of R-F Resin 55197-1-A

Band, (cm^{-1})	Assignment
3436	ν(O-H)
2964, 2908	ν(C-H)
1633, 1414	ν(C=C) "ring breathing"
1027, 1097	ν(C-O) symmetric and asymmetric stretch
865	δ(C-H) aromatic out of plane bending; 1,2,4,5-tetra-,1,2,3,4,5-penta-, or 1,2,4-tri-substituted ring
802	δ(C-H) aromatic out of plane bending; 1,2,3,4-tetrasubstituted ring

relectance IR techniques, the surface of R-F resin particles have been shown to have carbonyl functionality (ketone, quinone), which likely results from air oxidation of particle surfaces.

Samples of the R-F resin were analyzed by surface reflectance infrared analysis and by traditional transmittance infrared analysis to determine the relative effect of oxidation at the surface verses the bulk oxidation of the resin.

A photomicrograph of a BSC-187 resin is shown in Figure 4.11, along with the PNL-synthesized R-F resin 55197-2-A for comparison. The photomicrograph of the BSC-187 resin was taken through the optics of the infrared microscope at 10X magnification. As can be seen in this photo, thin portions of the resin are translucent, allowing for transmittance infrared analysis of that portion of the sample. Figure 4.12 contains the absorbance infrared spectrum (taken in transmittance mode) of the R-F resin. The basic features of this spectrum reveal strong absorbance due to the O-H stretching region at 3700-3000cm^{-1} region. Also apparent is the strong infrared absorbance bands due to the aromatic ring modes of the R-F resin material located at 1595cm^{-1} and ca. 1400cm^{-1}. There is a weak shoulder on the high energy side of the 1595cm^{-1} band which is in the approximate location for carbonyl bands, an expected air oxidation product of the R-F resin material. This band is largely occluded by the predominant aromatic ring bands.

A reflectance infrared spectrum was taken at the same location as the transmittance mode spectrum of the R-F resin material. In reflectance mode, the incident infrared signal is reflected off the surface of the sample and directed to the detector. In this manner, the surface structure of a sample can be probed preferentially over the bulk property of the sample. The reflectance spectrum is shown in Figure 4.12. As in the transmittance mode measurement, a prominent absorbance is observed for the O-H band in the 3700 - 3000cm^{-1} region. A band at 1732 cm^{-1} is also prominent feature of this spectrum. This is assigned to a carbonyl functionality which is due to the air oxidation of the R-F resin. The increase in intensity of this band in the reflectance mode measurement compared to the transmittance mode measurement indicated the oxidation of the resin is more prevalent at the surface of the resin. The bands associated with the aromatic ring modes are also observed in the reflectance measurement, but at a lower relative intensity than the carbonyl band.

4.2.3 Additional Structural Characterization of R-F Resin

Two of the PNL-synthesized resin samples (55197-2-A and 55197-2-B) were subjected to C and H elemental analysis. Resin 55197-2-A was found to be composed of 47.59% C and 3.92% H. Likewise, resin 55197-2-B was found to be composed of 47.30% C and 3.85% H. A theoretical unit of the resin polymer would be composed of the resorcinol ring with two methylene groups. Each methylene linkage is shared between two rings, therefore, one half, or one - CH_2- unit is added into the theoretical formula. One of the ring hydroxyl groups is in the potassium salt form giving a theoretical stoichiometry of $C_7H_5O_2K$. The calculated analysis for $C_7H_5O_2K$ gives: C, 52.48%; H, 3.15%; O, 19.97%; K, 24.40%. Addition of one unit of water gives a theoretical formula unit of $C_7H_7O_3K$ (C, 47.17%; H, 3.96%; O, 26.93%; K, 21.94%). The analysis seems to suggest that there is one mole of water per ring unit/ or potassium ion in these resins such that about 10% of the mass of the resin is composed of water. Elemental analyses for BSC-187 R-F resin in different ionic forms are presented in Table 4-6. These samples were also analyzed for alkali metal composition.

Resins 55197-2-A and 55197-2-B (20-50 mesh) were examined using microscopy. The deep red translucent particles were photographed and examined using SEM (magnification x175 to x700). These photos show particles with smooth glass-like surfaces that lack pore structure (Figure 4-13). In some cases there appear to be resin fines that adhere to the surface of larger particles, although some of these rough surface features may be due to local swelling of the resin surface. The two resins were also submitted for x-ray diffraction (XRD) analysis and found to have no distinguishing features (i.e., they were amorphous solids).

Figure 4-11. Photomicrographs of BS-187 R-F Resin Used for IR Analysis (top) and of PNL-Synthesized R-F Resin 55197-2-A, Showing 20 to 50 Mesh Particles (bottom)

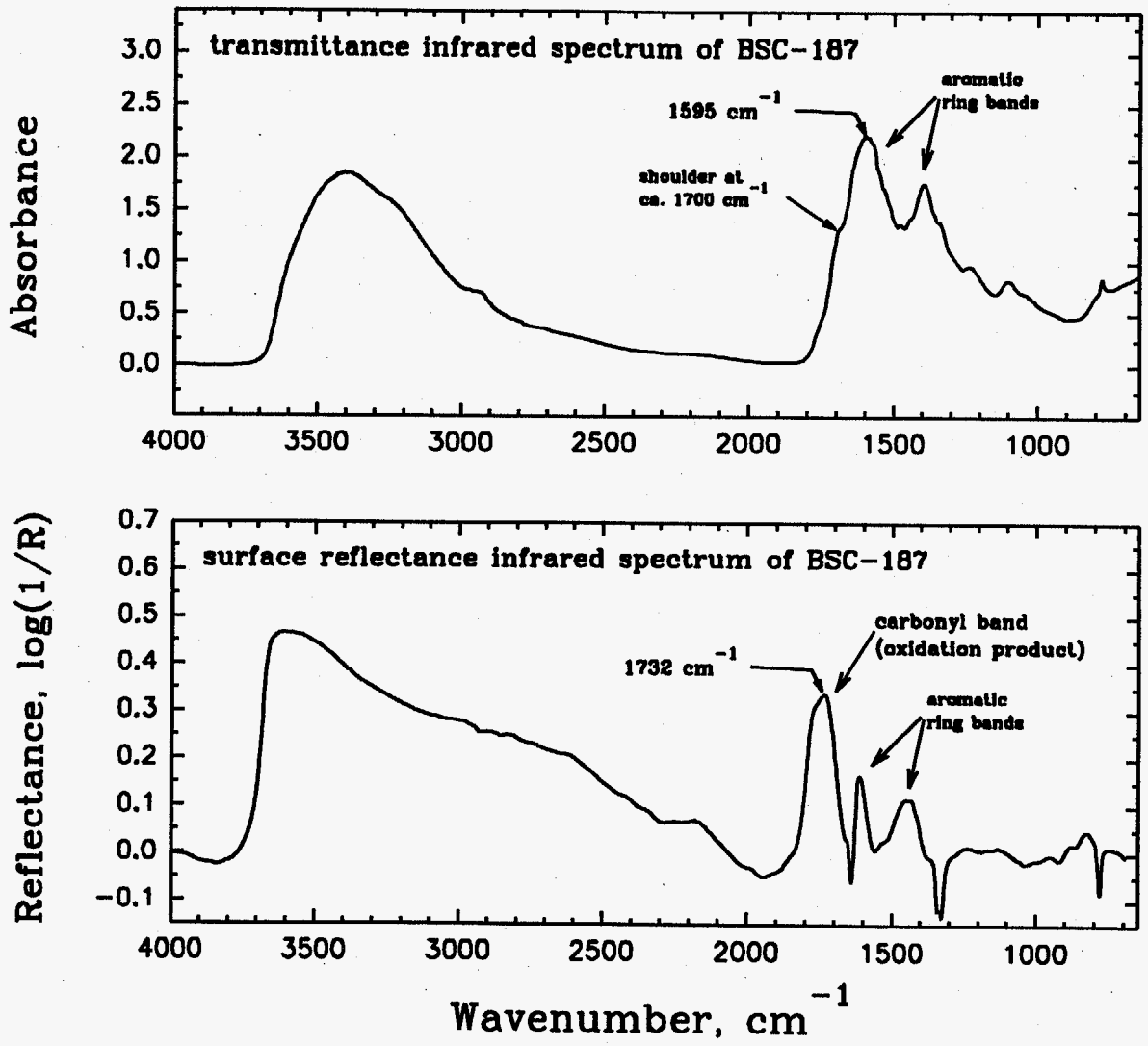

Figure 4-12. Infrared Spectra of BSC-187 R-F Resin. Spectra taken using FTIR microscope at 15X magnification. Top spectrum was taken in transmittance mode. Bottom spectrum was taken in reflectance mode.

Table 4-6. Elemental Analyses for BSC-187 in H^+, Na^+, K^+, and Cs^+ Forms

Form	% C Theory	% C Found	% H Theory	% H Found	% Na Theory	% Na Found	% K Theory	% K Found	% Cs Theory	% Cs Found
$H^{+(a)}$	68.85	66.81	4.95	4.70	--	0.097	--	<0.027	--	--
$Na^{+(b)}$	41.60	41.73	3.99	4.08	22.75	20.64	--	<0.051	--	--
$K^{+(c)}$	47.17	49.68	3.96	3.77	--	0.11	21.94	17.24	--	--
$Cs^{+(d)}$	30.91	33.56	2.59	2.27	--	0.30	--	--	48.86	43.39

(a) H^+ form prepared using formic acid

(b) Activated with 6M NaOH

(c) Stoichiometry: K^+/resorcinol (1/1)

(d) Activated with 2M CsOH

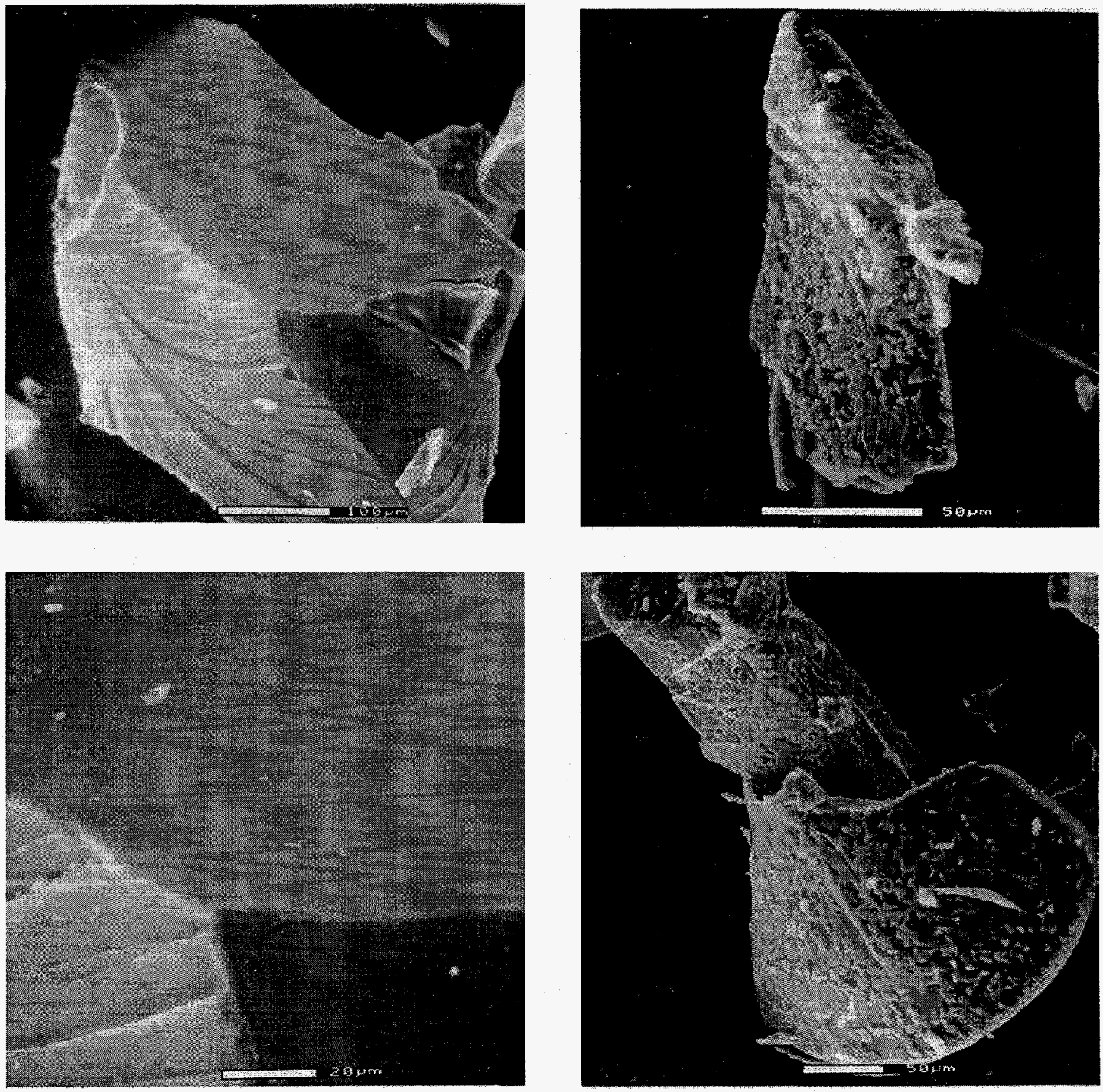

Figure 4.13. SEM Photomicrographs of PNL-Synthesized R-F Resin at (i) 100 um, (ii) 50 um, (iii) 20 um, (iv) 50 um Magnification. Note the presence of resin fines and/or swelling on the surface of the resin particles

BET analysis of resin 55197-2-B using nitrogen as the analysis gas was used to characterize surface area and pore structure of the resin [12]. The BET surface area was calculated to be 0.0668 m^2/g with a micropore volume equal to 8 x 10^{-6} cm^3/g. Average pore diameters were calculated to be 43.33 Å. This demonstrates that there is no macropore structure for the R-F resins, as expected for a microreticular condensation resin.

TGA/IR analysis of PNL resin 55197-2-A showed that the resin decomposes in a multistep process with initial mass loss occurring at 30 to 180 °C, which was shown to be water by the IR analysis. No other IR active gases were observed in the gases released from the sample between 60 and 105 °C. The organic portion of the resin begins to decompose at 110-135 °C with evolution of CO_2. Subsequently, there are four other stages of reaction decomposition which produce mainly CO_2 with some water at 140-210 °C, 220-430 °C, 430-560 °C, and 560-600 °C. In the final two stages there may be small amounts of methane that are produced from the decomposition reaction. Importantly, this study suggests that use of curing temperatures above 135 °C for preparation of R-F resin may be contraindicated since the resin chemically starts to decompose at these temperatures. Further experimentation on R-F resin in the acid form may help give insight into the stability of ionic versus nonionic forms of the resin.

In summary, elemental analyses support the proposed structure of the R-F resin. SEM and BET analysis show that the resin is microreticular. TGA/IR analysis shows that R-F resin has a low thermal stability with significant organic decomposition beginning around 135 °C. This suggests that curing temperatures of 135 °C and above should not be used for manufacture of R-F resin.

4.2.4 Characterization of Cesium-Loaded R-F Resin

The Cs loaded resins were characterized by comparison of elemental analyses to the solid-state ^{13}C and ^{133}Cs NMR spectra for each sample. The elemental analysis results are presented in Table 4-7. A description of the experimental procedure is given in Section 3.1.3.

Table 4-7. Elemental Analyses for Cesium-Loaded BSC-210 Resin Obtained from Contact with Various Ionic-Strength CsOH Solutions

Solution	Moles Cs (10^{-3})	C/Cs	%C Theory	%C Found	%H Theory	%H Found	%Cs Theory	%Cs Found	% Moisture
A	1.01	121.9	64.93	58.43	4.68	5.09	5.06	5.30	10.80
B	3.12	36.9	57.29	48.70	5.40	4.65	13.86	14.64	11.79
C	9.33	14.7	44.16	33.07	3.39	4.28	31.80	24.97	19.37
D	15.9	11.4	35.24	31.05	2.84	3.68	43.28	30.06	14.68
E	62.5	8.5	19.91	24.95	1.90	4.47	63.03	32.35	27.26
F	250	6.2	19.91	19.05	1.90	2.82	63.03	34.04	8.39

Figure 4-14 shows ^{133}Cs NMR as a function of the cesium concentration of the contact solution. The CsOH solutions were prepared such that the amount of cesium ion would be stoichiometrically equivalent to exchange with 2.5% (A), 7.6% (B), 22.7% (C), 38.8% (D), 152.% (E), and 609.8% (F) of the theoretical number of ion-exchange groups present in the resin (assuming all cesium ions are exchanged onto the resin). The ^{133}Cs NMR shows that a weak broad cesium resonance appears at -93 ppm (relative to CsCl standard) for resin contact with solution A. Solution C, shows the resonance at -93 sharpens, and for solution D, the resonance at -93 ppm has started to show resolution of two additional resonances. For R-F resin contacted with solution E, where theoretically all the exchange sites are associated with cesium ion (the resin is just past the saturation point), different environments for the cesium ion in the resin become very apparent as peaks at -93, -202.8 and -172.8 ppm appear well resolved. The differences in these sites may be correlated to the differences in pK_a values for the two hydroxyl groups in each resorcinol unit of the polymer. As the amount of CsOH in the contact solutions is increased, the pH of the solution increases with the result that both hydroxyl groups of the resorcinol unit are deprotonated and available for ion-exchange. When the resin is contacted with solution F, which contains at least 6 times the theoretical number of exchange sites, resolution of three distinct environments for the cesium ion has given way to a single resonance of -173 ppm. Elemental analyses show that there is far less cesium ion in R-F resin contacted with solution E and F than would be expected if the resin were saturated with cesium. The simplification of the ^{133}Cs NMR spectrum to a single resonance may indicate a higher mobility of the cesium ion as the resin becomes saturated. The mobility of the cesium ion within the resin is possible because of the free water present in the resin.

^{13}C NMR spectra for the Cs^+ loaded resins are shown in Figure 4-15. These spectra show that high ion loading results in increasing complexity of the ring hydroxyl carbon (*ipso)* resonance at 150-165 ppm. The appearance of the resonance at about 165 ppm at higher cesium loading (lower C/Cs ratio) reflects the substitution of different hydroxyl sites, perhaps due to ionization of a second hydroxyl group on the resorcinol ring. These results directly parallel results of ^{13}C NMR spectra of sodium-loaded R-F resin. For R-F resin contacted with 2 M NaOH, the largest *ipso* resonance is at 154.5 ppm, but for R-F resin contacted with 6 M NaOH, the more intense resonance among the phenolic carbons also appears at about 165 ppm.

In the above samples, the ionic strength of the CsOH solutions was varied, which may have contributed to the differences in the spectra. To explore the effect, R-F resin was contacted with solutions of constant ionic strength. These solutions were prepared by the varying amounts of CsOH and NaOH, while keeping the hydroxide ion concentration constant. The ^{13}C NMR spectra are shown in Figure 4-16. No significant difference in the ^{13}C NMR for the *ipso* carbons is observed when compared to the spectra for the cesium hydroxide only case (Figure 4-15). Approximately the same number of ion-exchange (hydroxyl) sites are occupied in each resin sample, but with differing amount of sodium or cesium ion. The ^{133}Cs NMR spectra are shown in Figure 4-17, and are very similar to those observed for the varied ionic strength case (Figure 4-14), although there is a dramatic change in going from a high $[Na^+]$ solution to the Cs^+ only solution (Table 4-8). When the contact solution is composed of 100% cesium ion, without the presence of sodium ion, the chemical shift of the cesium is again observed at the frequencies seen previously for the varied ionic strength case.

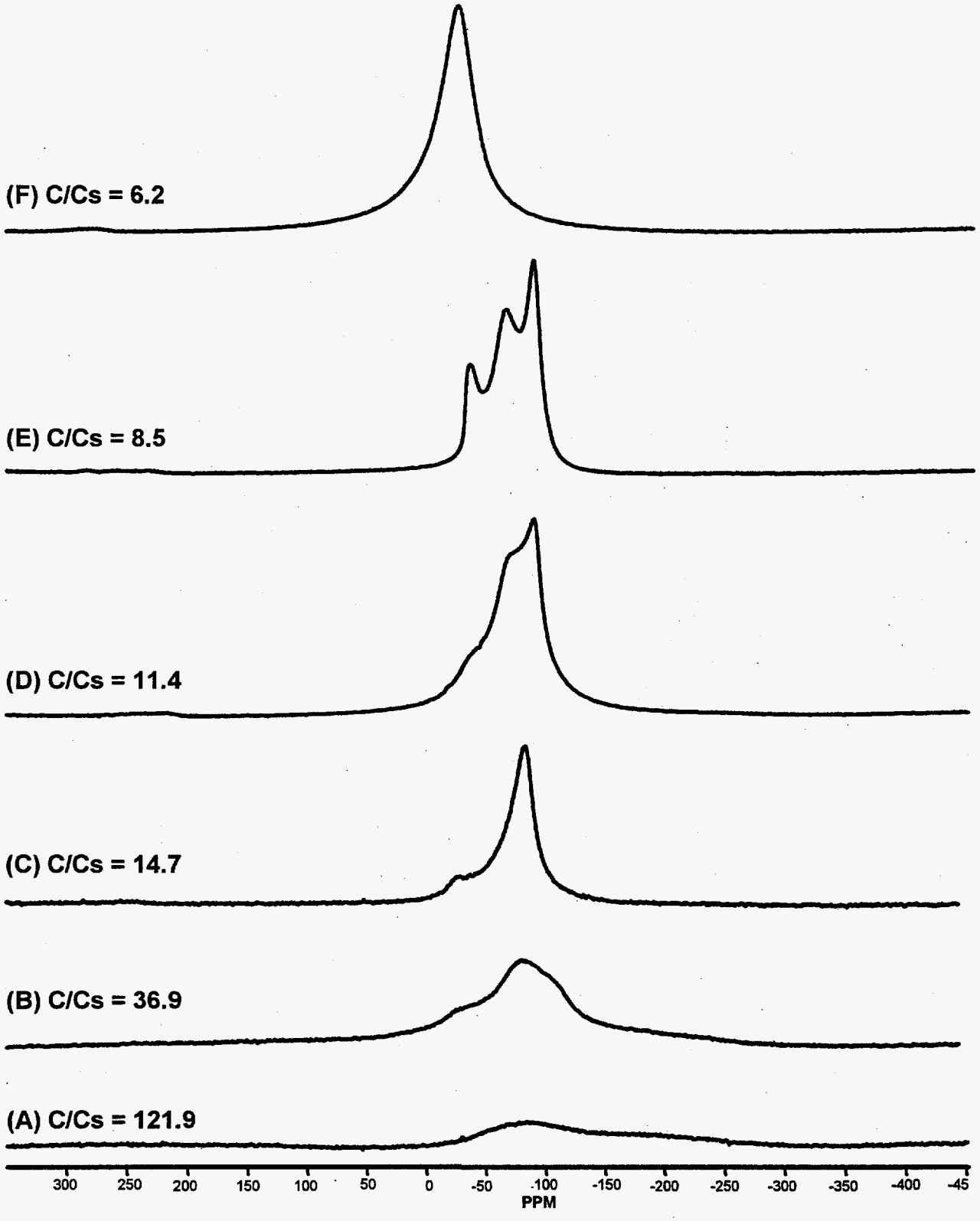

Figure 4-14. ^{133}Cs NMR Spectra of BSC-210 Contacted with Varied Ionic Strength CsOH Solutions

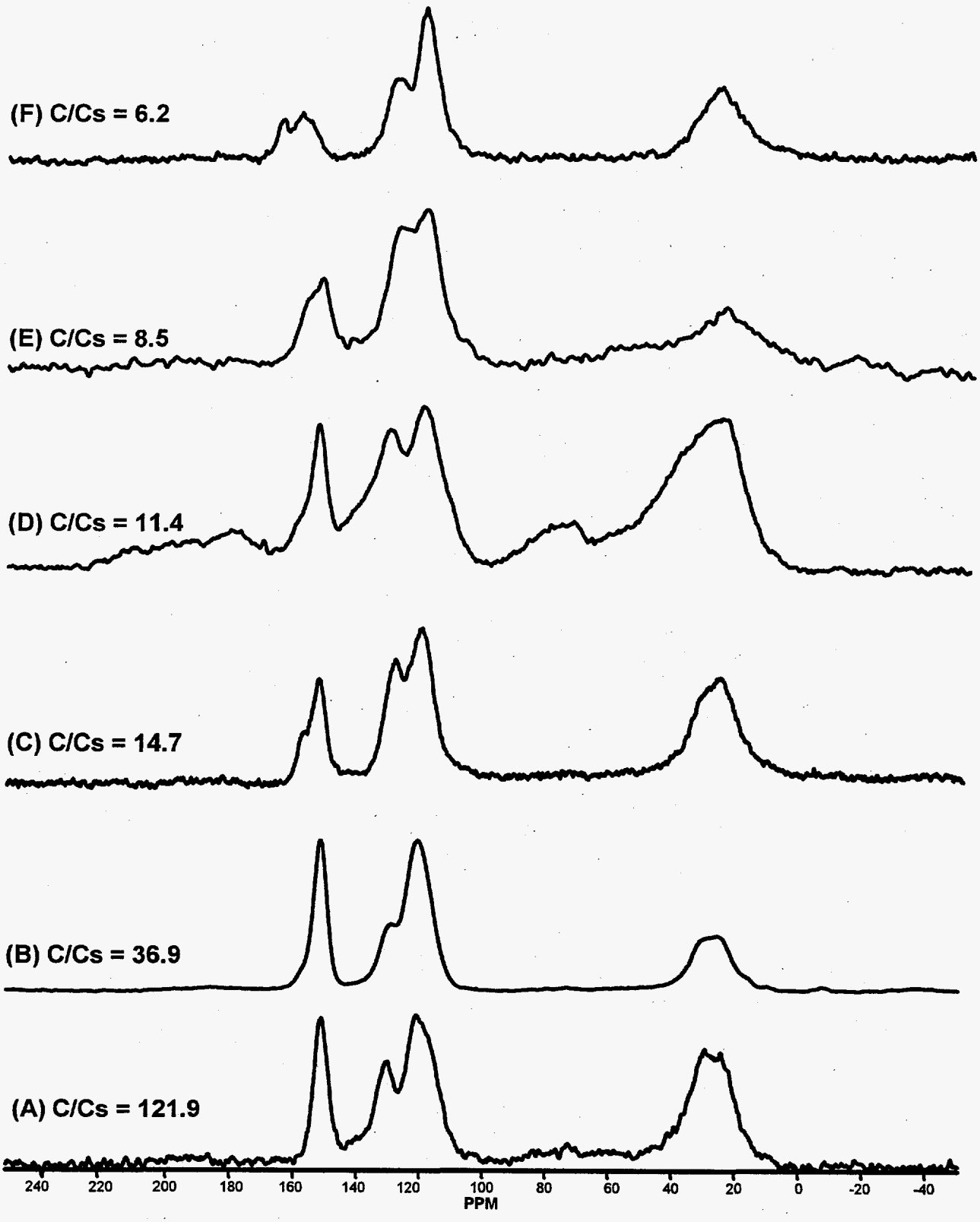

Figure 4-15. ^{13}C NMR of BSC-210 Contacted with Varied Ionic Strengths of CsOH Solutions

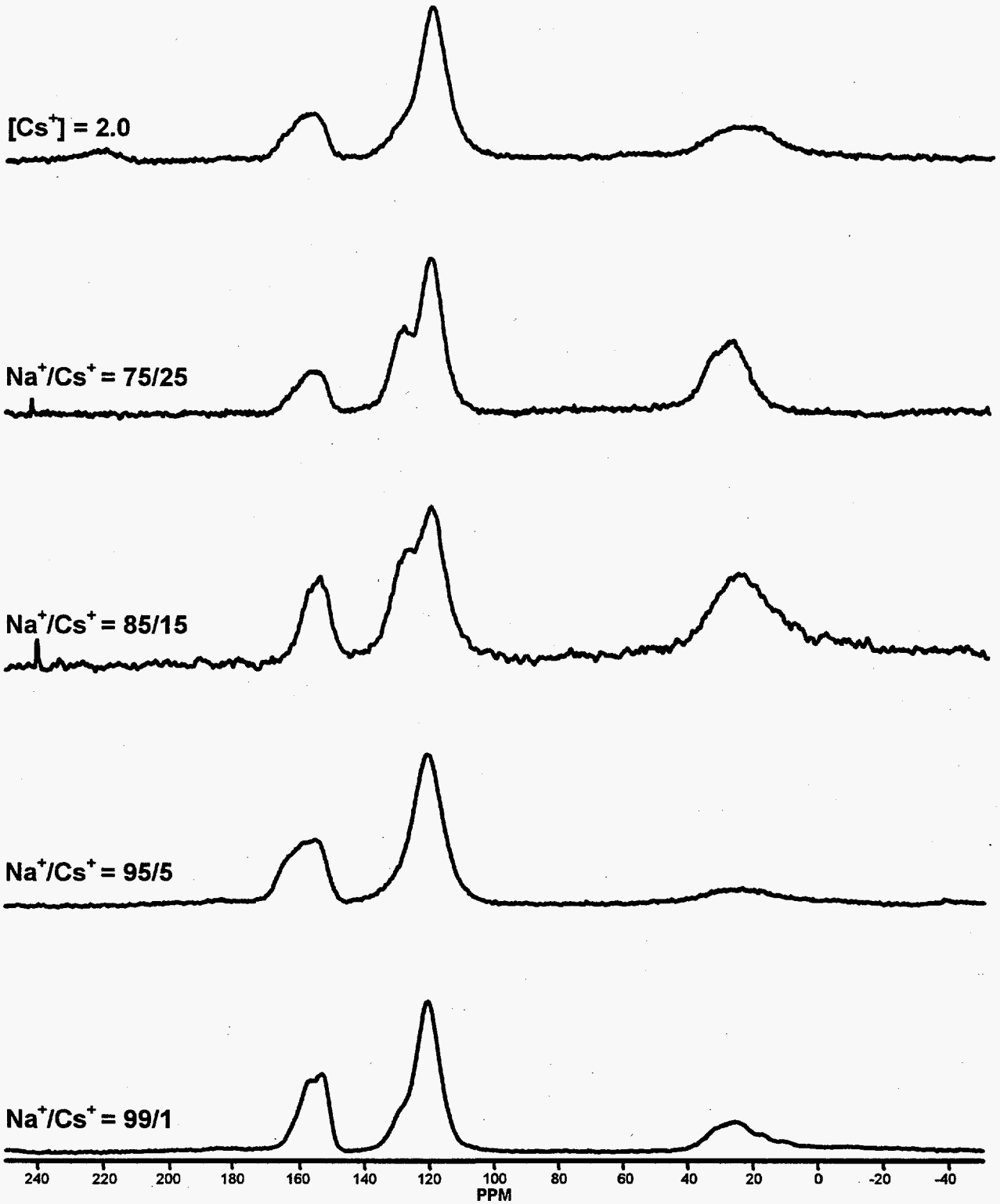

Figure 4-16. ^{13}C NMR of BSC-210 Contacted with Constant Ionic Strength Na^+/Cs^+ Solutions

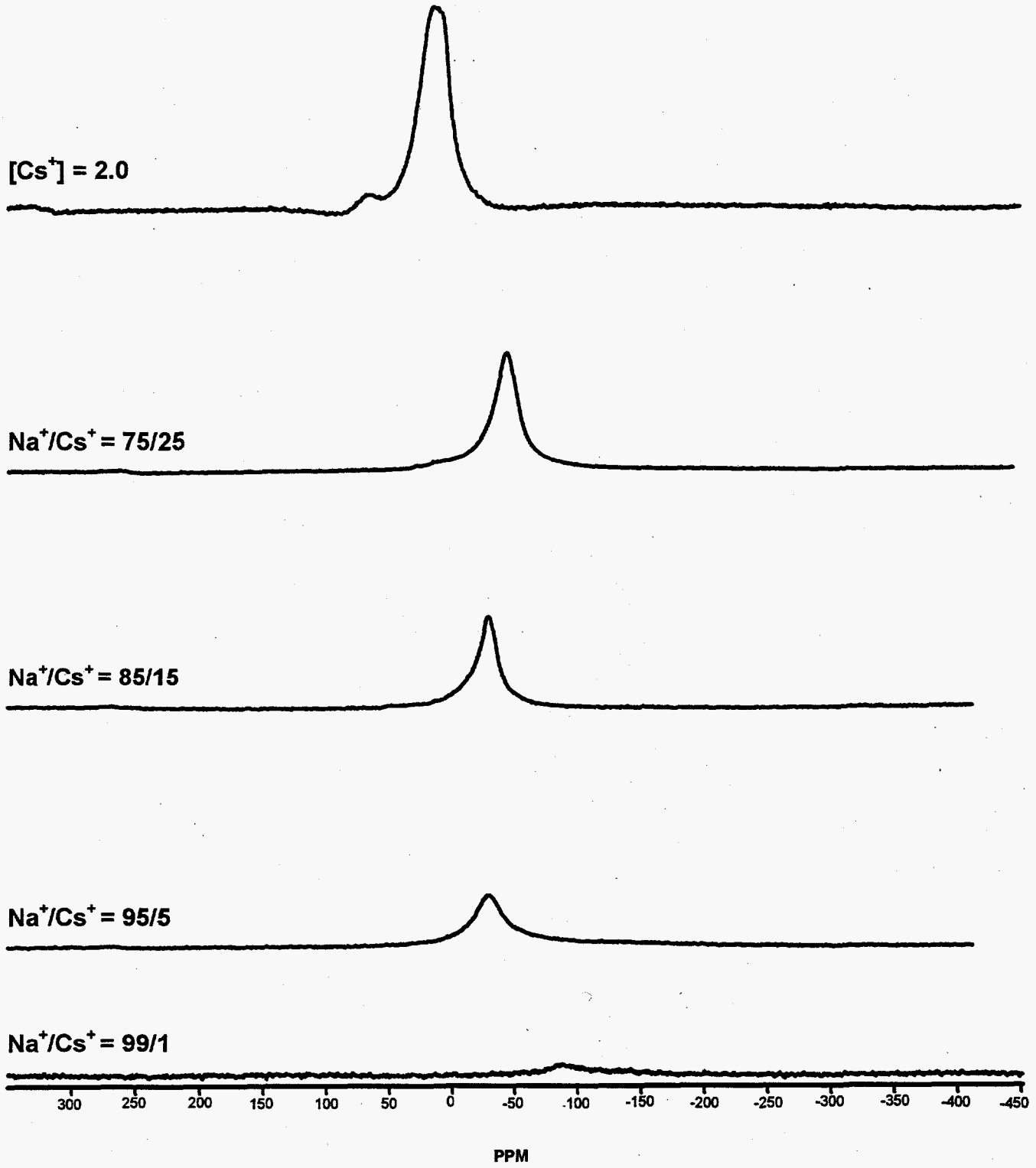

Figure 4-17. ^{133}Cs NMR Spectra of Constant Ionic Strength Na^+/Cs^+ Solutions

Table 4-8. Elemental Analyses of BSC-210 Contacted with Solutions of Constant 2M OH^- Ionic Strength, but Varying Na^+/Cs^+ Ratios

Na^+/Cs^+ (%)/(%)	%C Theory	%C Found	%H Theory	%H Found	%Cs Theory	%Cs Found	%Na Theory	% Na Found
99/1	46.64	46.81	4.44	4.72	1.33	1.57	12.64	12.59
95/5	45.53	44.13	4.34	4.38	3.60	11.55	11.84	11.71
85/15	42.97	40.36	4.09	3.38	10.2	20.52	10.0	7.27
75/25	40.68	35.85	3.87	3.13	16.10	26.33	8.35	6.53
Cs^+=0/100	19.91	27.31	1.90	2.73	63.03	45.49	--	0.031

4.3 CS-100 (Phenol-Formaldehyde) Resin

CS-100 is a phenol-formaldehyde resin for which ^{13}C NMR spectra (Figure 4-18) suggests a significant presence of ether groups by resonances in the 50-75 ppm region. ^{13}C Bloch Decay NMR for CS-100 (for which carbon resonances may be accurately integrated) shows the ratio of ether carbons to bridging methylene carbons to be 1.00 to 2.33, respectively. The elemental analysis results for CS-100 in both H^+ and Na^+ forms, Table 4-9, do not support a structure in which there is significantly more crosslinking than observed for R-F resin. When taking into account the ether groups in the ratios suggested by the Bloch Decay ^{13}C NMR data, a polymeric structure composed of the two basic units, as pictured in Figure 4-19 can be envisioned. The significant differences between the theoretical and observed values for carbon analysis of CS-100 may be due to resin oxidation caused by incorporation of *p*-toluic acid in the polymer, which is a modifier added by the manufacturer. However, there are no carboxylate or carboxylic acid carbon resonances observed in the ^{13}C NMR spectra as evidence for incorporation of *p*-toluic acid into the polymer resin. The calculated values for carbon and hydrogen in Table 4-9 are based upon the structures shown in Figure 4-19 in the ratio of 54.8% to 45.2% of A and B, respectively.

Table 4-9. Elemental Analyses of CS-100 in H^+ and Na^+ Ionic Forms

CS-100 Ion Form	% C Theory	% C Found	% H Theory	% H Found	% Na Theory	% Na Found	% K Found
H^+ form	79.85	72.63	5.53	5.34	--	0.058	<0.030
Na^+ form	68.53	63.23	5.10	4.53	8.15	5.07	<0.042

Infrared analysis of the resin (KBr pellet) gave some corroboration to the structures shown above. The ν(C-O) bands for the aromatic ring carbon to hydroxyl group stretch were observed at 1137 and 1021 cm^{-1} (symmetric and asymmetric stretch), while a significant aromatic carbon to oxygen stretching frequency was observed at 1208 cm^{-1} which would arise from the presence of $-OCH_3$ or related ether groups attached to the aromatic ring. In the aromatic C-H deformation region, a relatively strong band is observed at

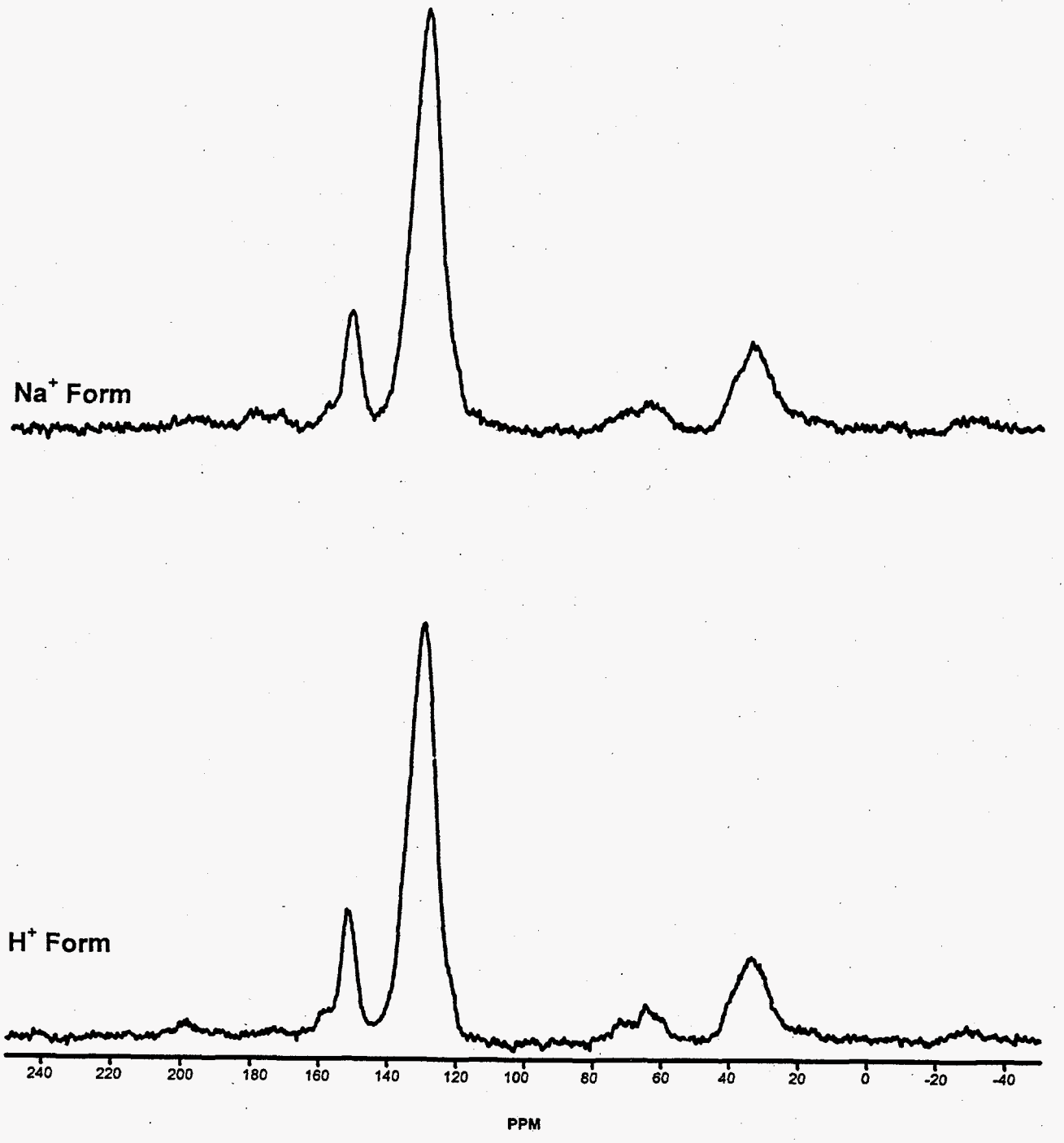

Figure 4-18. ^{13}C NMR of CS-100 in Na^+ and H^+ Forms

A B

Figure 4-19. The Two Structural Components of Duolite CS-100 Resin: A - 54.8%; B - 45.2%

observed at 799 cm^{-1} while a weaker band occurs at 876 cm^{-1}. The band at 799 cm^{-1} may arise from the familiar 1,2,3,4-tetrasubstituted ring system observed for R-F resin. However, this pattern would be inconsistent with the known reactivity of the phenolic ring (giving metasubstitution). When the 799 and 876 cm^{-1} band are taken together, a 1,2,4-trisubstituted ring system is indicated and is consistent with the NMR data and the structures presented in Figure 4-19. R-F resin shows very little, if any absorption at 876 cm^{-1}. The presence of a small amount of this band in R-F resin would be indicative of 1,2,4-trisubstitution of the resorcinol ring, or rather the presence of non-crosslinked polymer units.

4.4 Oxidation Studies of R-F and CS-100 Resins

Resorcinol and its derivatives are oxidized to give *p*-bisquinones under alkaline conditions [18]; therefore, the likelihood that the observed variation in the performance of R-F resin (based on K_d's) was due to resin oxidation required further examination. These studies indicate that there is modest incorporation of oxygen into the resin under normal atmospheric conditions which result in the formation of ketone and quinone structures within the polymer resin that produce concomitant decreases in the number of exchange sites which in turn lower the cesium K_d's.

Figure 4-20 shows the effects of exposure of R-F resin to alkaline media, by correlation of ^{13}C NMR spectra with K_d's. In the spectrum shown in Figure 4-20(a), the ^{13}C solid-state NMR spectrum of BSC-187 is shown, and indicates that there has been little or no oxidation to the structure of the resin. The K_d value for this resin is 3700 mL/g. In contrast, the spectrum shown in Figure 4-20(b) shows a sample of BSC-187 resin that has severely degraded after exposure to 2M NaOH solution. After a 6-month exposure time, the K_d dropped from 3700 to 195 mL/g. The ^{13}C NMR spectrum reveals severe oxidation of the resin to ketone, quinone, and methylene bridgehead carbons substituted with oxygen. Thus, the long term effects of exposure of R-F resin to alkaline media show that performance is degraded through oxidation of the resin to give structures (ketones, quinones), which destroy exchange sites. This example clearly shows the usefulness of ^{13}C NMR for use as a technique to monitor quality of the R-F resin.

To quantify the amount of resin oxidation, controlled oxidation of R-F resin was observed by measuring the oxygen uptake of the polymers dispersed in 1 M NaOH, 6 M NaOH, and NCAW simulant supernate. The time-dependent oxygen uptake data is shown in Figure 4-21. The highest rate of oxidation was found with R-F resin in 1M NaOH. Higher base concentrations (6 M NaOH, NCAW supernate) exhibited lower oxygen uptake by R-F resin. CS-100 generally exhibited slower oxygen uptake, with amounts that were one-third or less than observed for R-F resin.

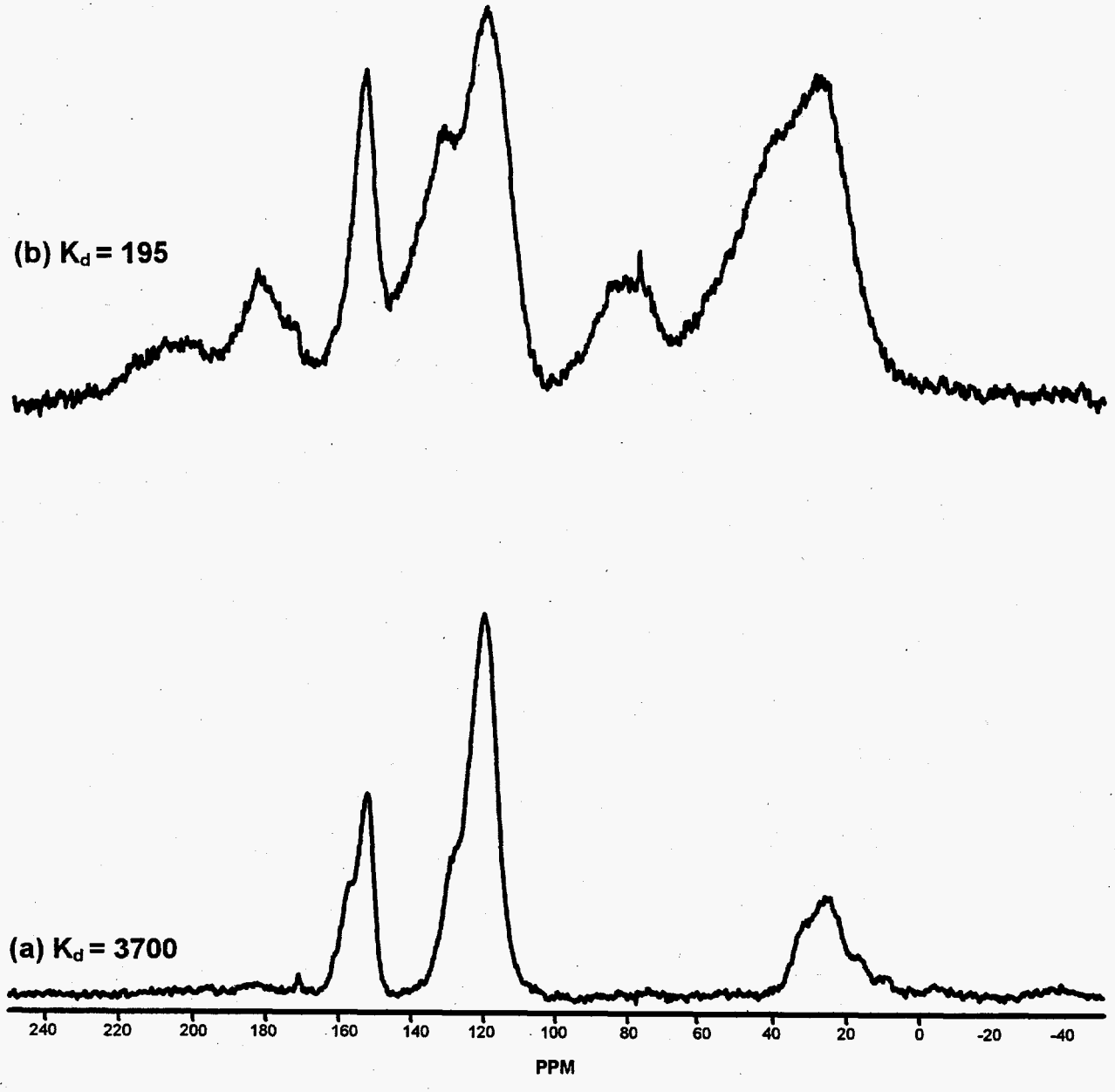

Figure 4-20. ^{13}C NMR of (a) BSC-187 (K^+ Form, Dry) as Received (b) BSC-187 After Being Contacted for Six Months with 2M NaOH in the Presence of Air

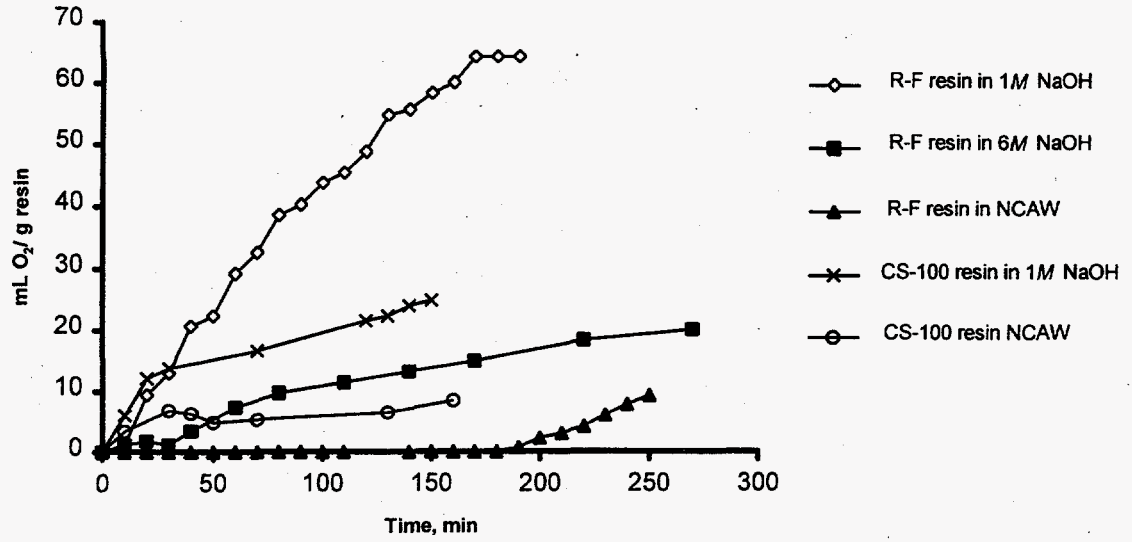

Figure 4-21. Oxidation Kinetics of R-F and CS-100 Resins in Aqueous Media

The rates of oxygen uptake may be affected by factors such as oxygen solubility in the aqueous phase and the amount of resin swelling (recall that more dilute external solutions favor increased resin swelling). However, the significantly faster uptake of oxygen by R-F compared to CS-100 underscores the more vulnerable nature of R-F resin to oxidative degradation. For R-F resin contacted with 1M NaOH solution, the observed level of oxidation at 200 min corresponds to uptake of about one oxygen atom for every three polymer rings, a significant level of oxidation. By contrast, no oxygen uptake was observed for the dry resin (K^+ form).

To further examine the structural effects of oxidation, a sample of BSC-210 resin was purged with air for 70 h in the presence of 1M NaOH. Figure 4-22 shows ^{13}C NMR spectra of the resin before and after air purge. Profound structural transformation is apparent. A substantial fraction of the aromatic carbons have been converted to carbonyl functional groups as indicated by the decrease in intensity of the *ipso* (-OH) aromatic carbon resonances at 145-160 ppm with a concomitant increase of ketone, quinone, and carboxylate signals at 165-230 ppm. Resonance in the 80-100 ppm region also shows that oxidation of the methylene groups has occurred. Note that spectrum 4-22 (b) exhibits a much lower aromatic/ aliphatic structure ratio; that is, the total peak area ratio for the region 100-220 ppm/ area of region 10-100 ppm compared to Figure 4-22 (a). This is primarily due to the high concentration of aromatic free radicals in the resin. The presence of high concentrations of aromatic radicals suppresses the detection of aromatic structure; therefore, the aromatic/aliphatic structure ratio is distorted. However, the substantial fraction of oxidized structure (165-220 ppm) qualitatively represents extensive oxidation.

The BSC-210 resin was oxidized using exposure to pure oxygen for variable lengths of time. The resin samples were first converted from the potassium to the acid form. Samples of about 2.5 g were placed in 1M NaOH and purged with oxygen for 0.5, 2.5, and 19.5 h. The samples were examined by elemental analysis and in some cases by ^{13}C NMR (beginning and 0.5 h). Elemental analysis are presented in Table 4-10. Table 4-10 shows a small monotonic decrease in the carbon/oxygen ratio, indicating modest incorporation of oxygen in the resin.

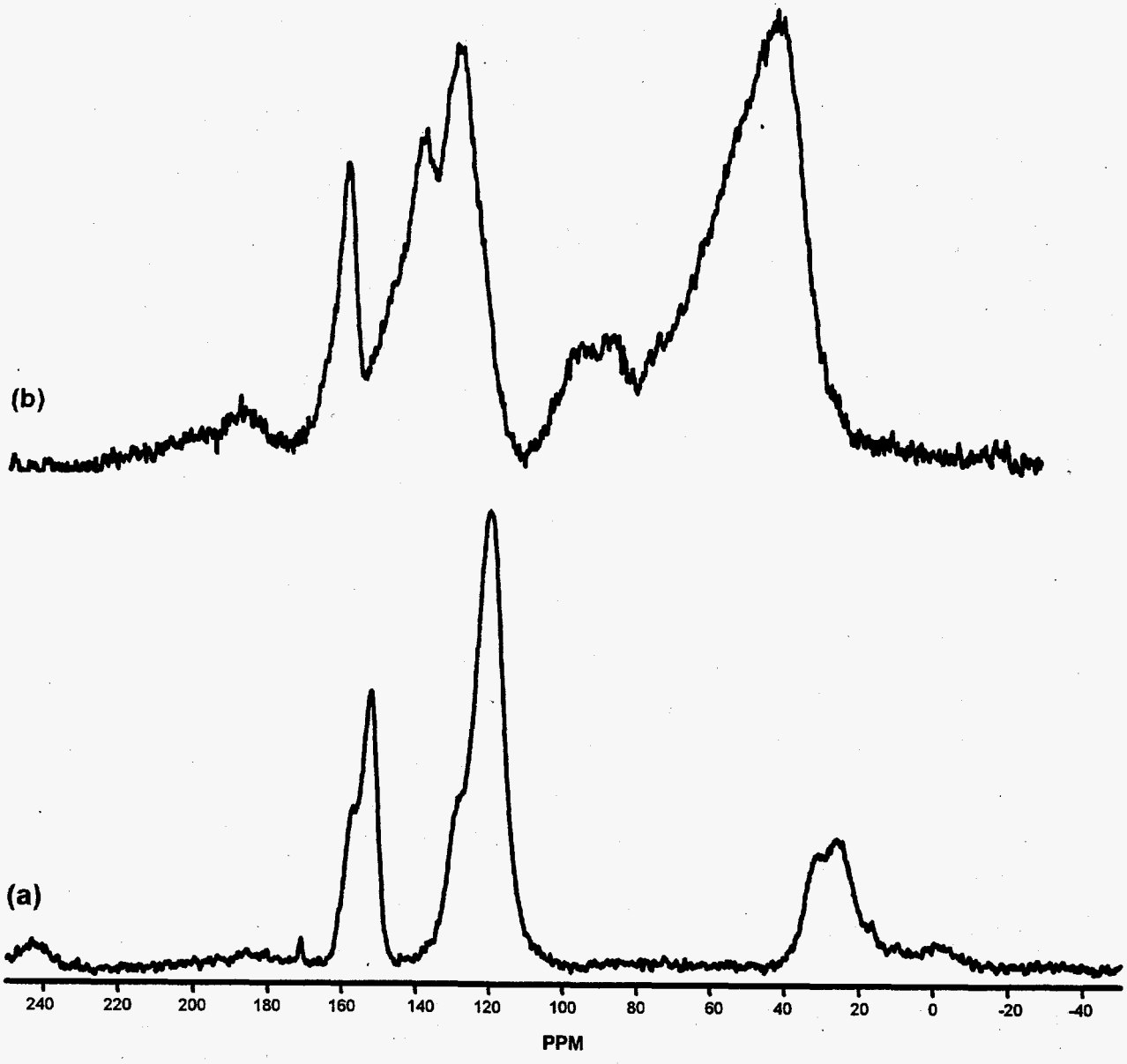

Figure 4-22. ^{13}C NMR BSC-210 (a) Before with Alkaline Solution (b) After Being Contacted with 1M NaOH for 70 h Under Air Purge

Table 4-10. Elemental Analysis of BSC-210 Resin Purged with Air for Varied Lengths of Time

Sample Time	% C	% H	% O	C/O
0 hours	63.06	4.77	27.54	7/2.18
0.5 hours	63.36	4.63	27.45	7/2.28
2.5 hours	63.81	4.60	28.15	7/2.32
19.5 hours	63.66	4.58	28.78	7/2.37
Unhydrated (theory)	68.85	4.95	26.2	7/2.0
Monohydrated (theory)	60.0	5.75	34.25	7/3.0

Several considerations must be taken into account in interpreting the data. First, the resins were reconverted to the acid form. The result is that highly oxygenated materials that become water soluble are removed, altering the C/O ratio. Second, the percentages of the elements obtained from analysis (Table 4-10) add up to about 96%, indicating some residual ash. The resin may incorporate some strongly associated water of hydration not removed under vacuum. Finally, the resin may have less than the theoretical number of bridging methylene units, reducing the percentage of carbon while increasing the percentage of oxygen. The actual analyses for carbon and oxygen are intermediate to the theoretical values calculated for monohydrated and unhydrated resin. Nevertheless, modest amounts of additional oxygen are likely incorporated into the polymer resin. Such a scenario suggests conversion of the phenolic function to quinones and possible consumption of oxygen to form oxidatively coupled rings. For the latter, some oxygen is eliminated as water rather than being incorporated into the polymer structure.

4.5 Radiolytic Stability of R-F and CS-100 Resins

Duolite CS-100 and BSC-210 resins were subjected to gamma radiolysis in the presence of both non-flowing NCAW waste simulant supernate and flowing NCAW waste simulant supernate regimes, at doses of 1×10^8 - 1×10^9 Rad over a period of five months. When R-F resin was subjected to (a) non-flow conditions without gamma radiolysis under nitrogen atmosphere, no oxidation of the resin occurred. However, for cases of (b) no flow, gamma irradiation, (c) flow, no irradiation, or (d) flow and irradiation, significant levels of oxidation were apparent. This is illustrated in Figure 4-23, which compares the resin under various irradiation conditions. For CS-100, the amount of quinone and carboxylate carbons slightly more than doubled (assessed using ^{13}C NMR) over the low initial value in each case. However, little overall structural transformation occurred with this resin, reflecting a lower degree of vulnerability of the resin to radiolytic-induced degradation compared to R-F resin. Figures 4-23 through 4-30 show typical NMR results from these studies. For R-F resin, there is a notable increase of the region 162 to185 ppm, which is attributed to the presence of quinone and carboxylate carbons. Thus, moderate degradation of R-F resin occurred during batch radiolysis tests and the control experiments while CS-100 resin showed little susceptibility to radiolytic-inducted degradation.

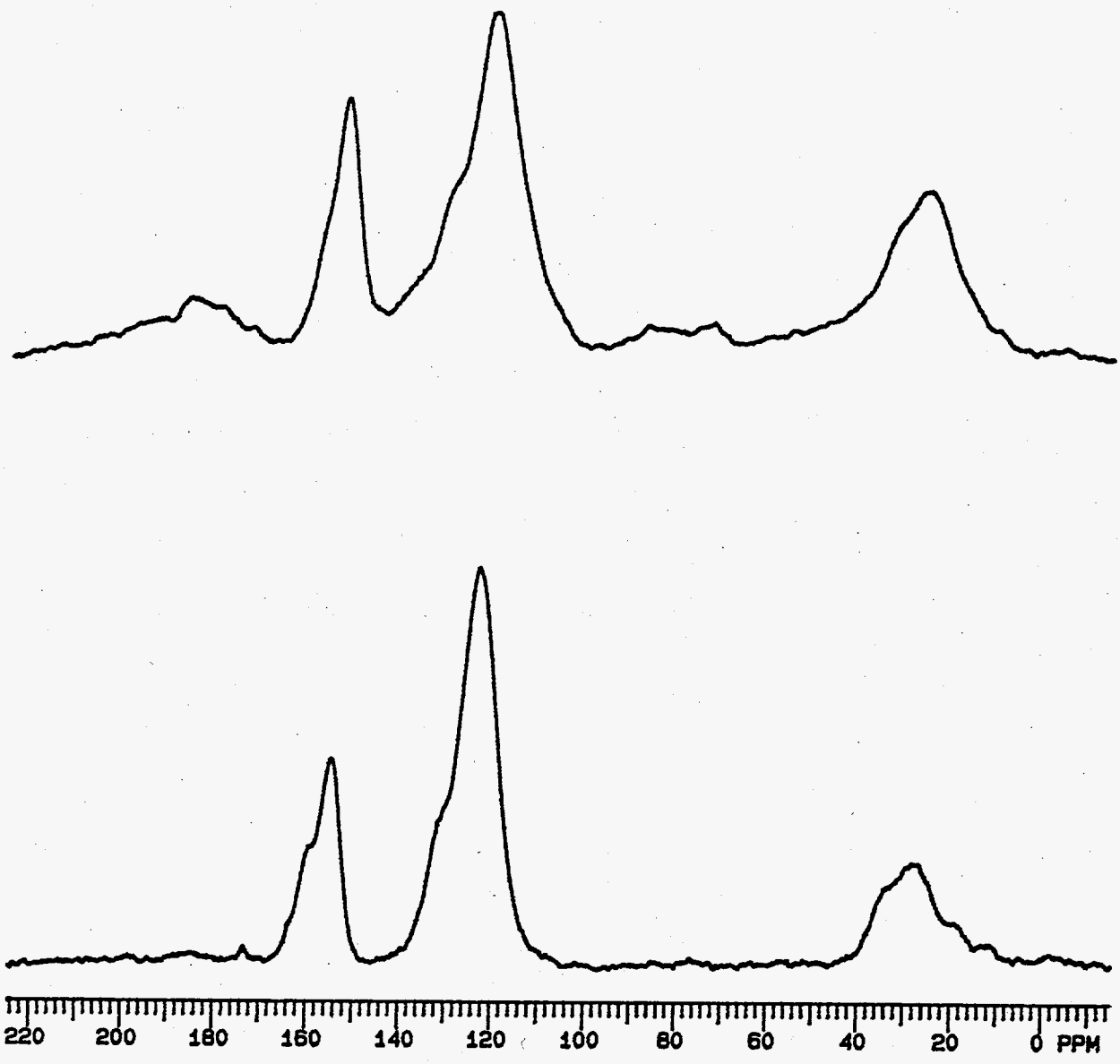

Figure 4-23. ^{13}C NMR Spectra of BSC-210 Resin Obtained at 12 kHz MAS for Conditions of No Gamma Irradiation with Flowing NCAW Waste Simulant (top) Compared to Standard BSC-210 Resin (bottom)

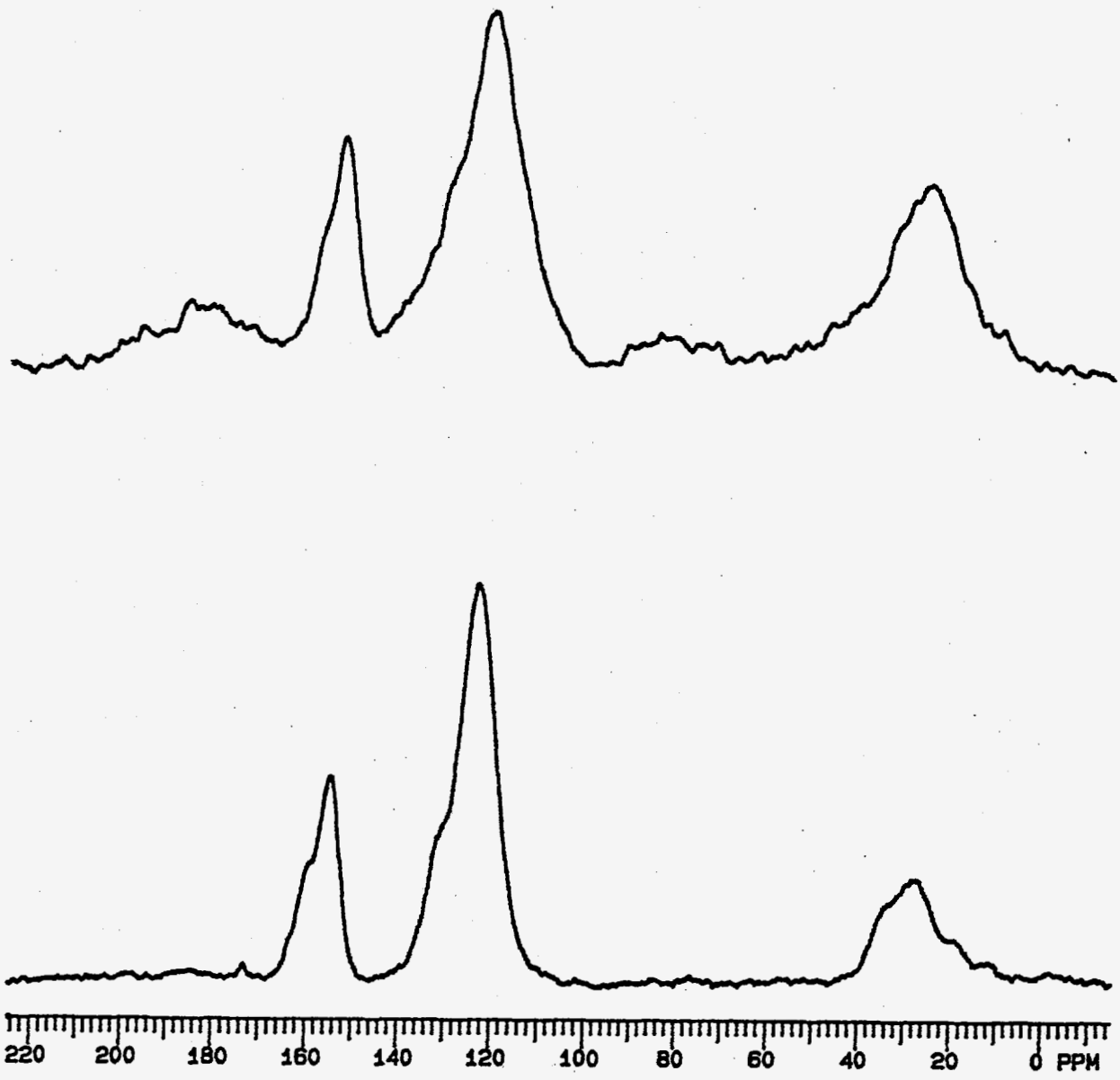

Figure 4-24. ^{13}C NMR Spectra of BSC-210 Resin Obtained at 12 kHz MAS for Conditions of Gamma Irradiation (1 x 10^9 R) with Flowing NCAW Waste Simulant (top) Compared to Standard BSC-210 Resin (bottom)

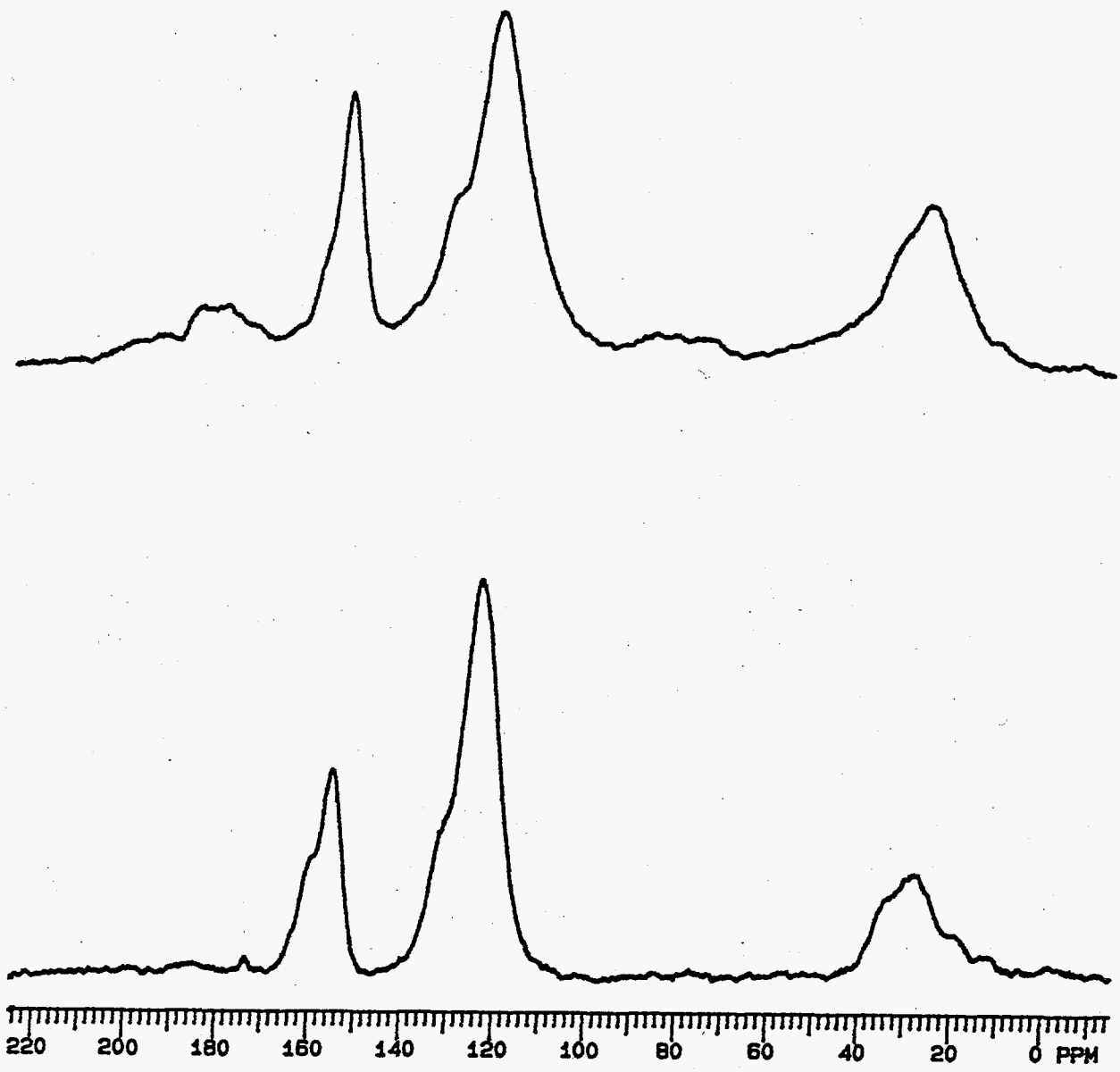

Figure 4-25. ^{13}C NMR Spectra of BSC-210 Resin Obtained at 12 kHz MAS for Conditions of Gamma Irradiation (1 x 10^9 R) with Static NCAW Waste Simulant (top) Compared to Standard BSC-210 Resin (bottom)

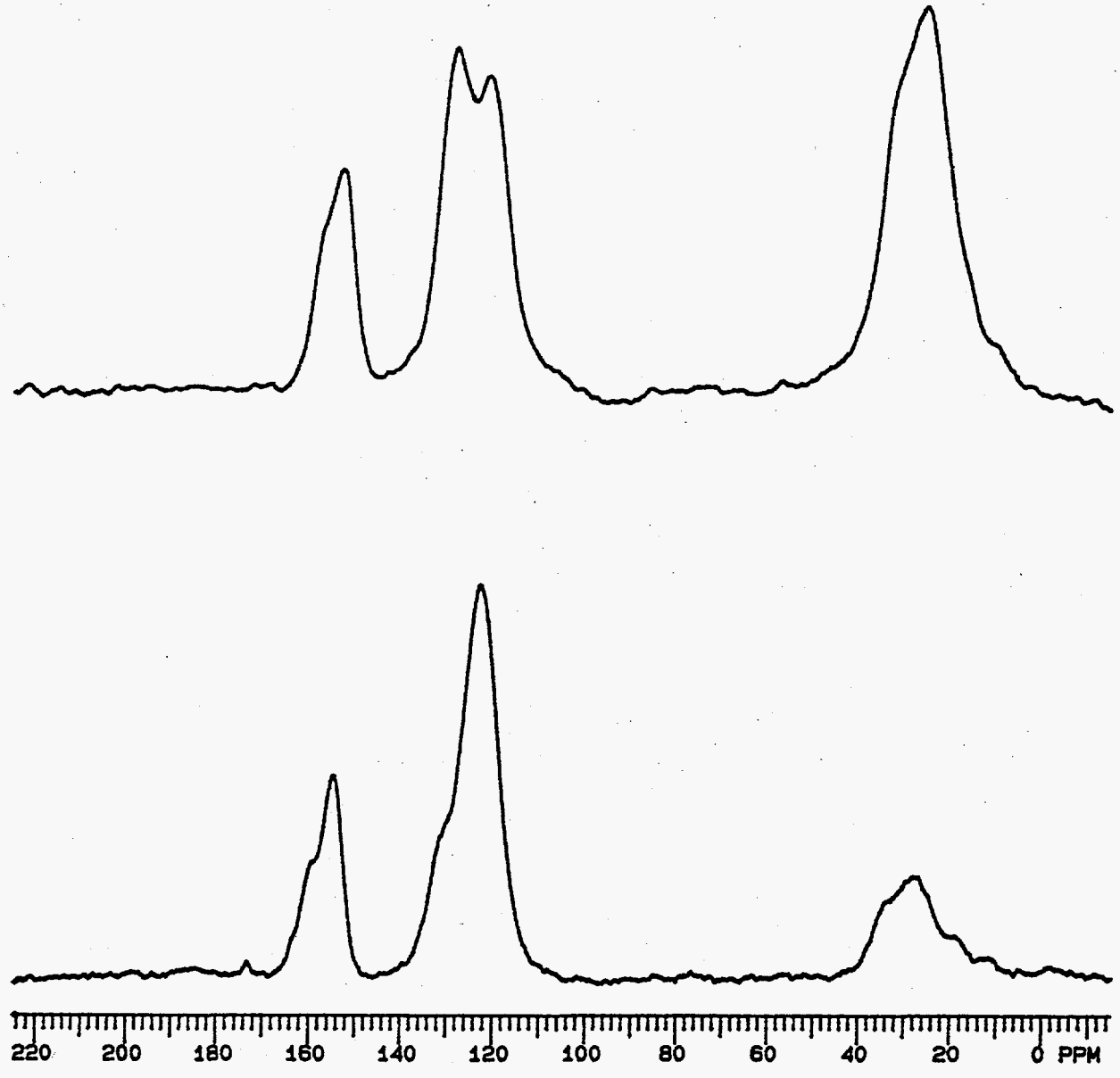

Figure 4-26. ^{13}C NMR Spectra of BSC-210 Resin Obtained at 12 kHz MAS for Conditions of No Gamma Irradiation with Static NCAW Waste Simulant (top) Compared to Standard BSC-210 Resin (bottom)

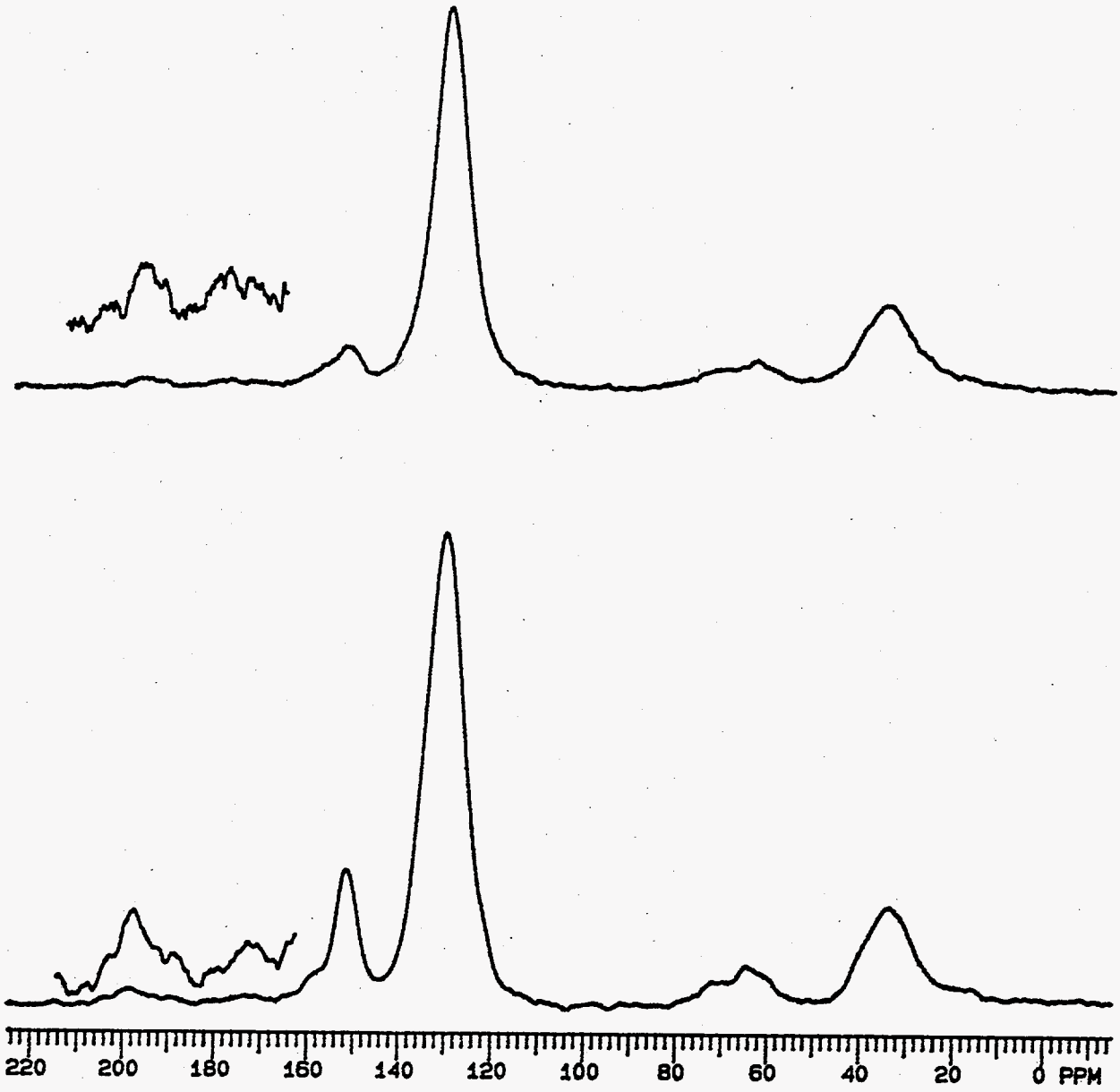

Figure 4-27. ^{13}C NMR Spectra of CS-100 Resin Obtained at 12 kHz MAS for Conditions of No Gamma Irradiation with Flowing NCAW Waste Simulant (top) Compared to Standard CS-100 Resin (bottom)

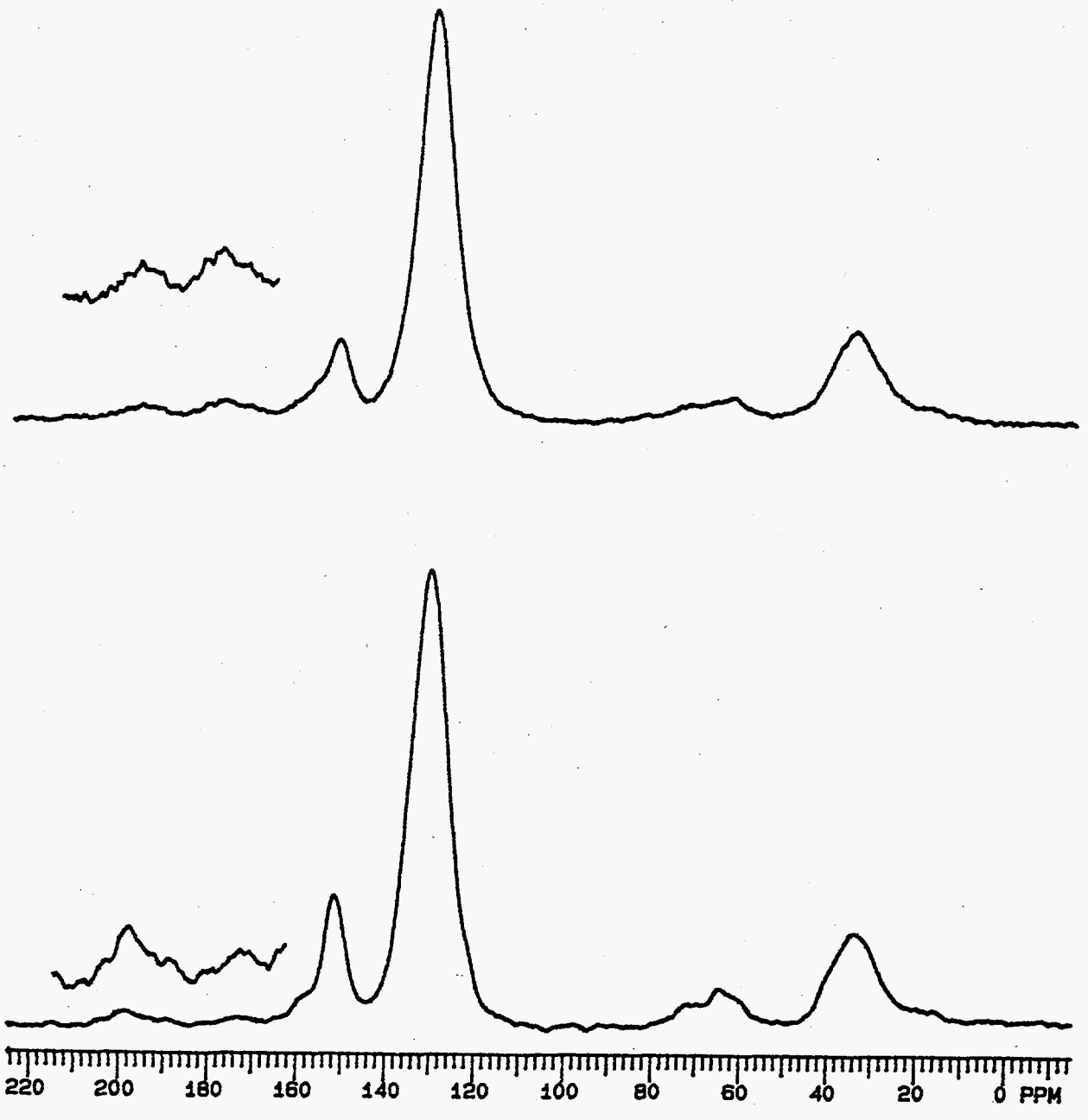

Figure 4-28. ^{13}C NMR Spectra of CS-100 Resin Obtained at 12 kHz MAS for Conditions of Gamma Irradiation (5×10^8 R) with Flowing NCAW Waste Simulant (top) Compared to Standard CS-100 Resin (bottom)

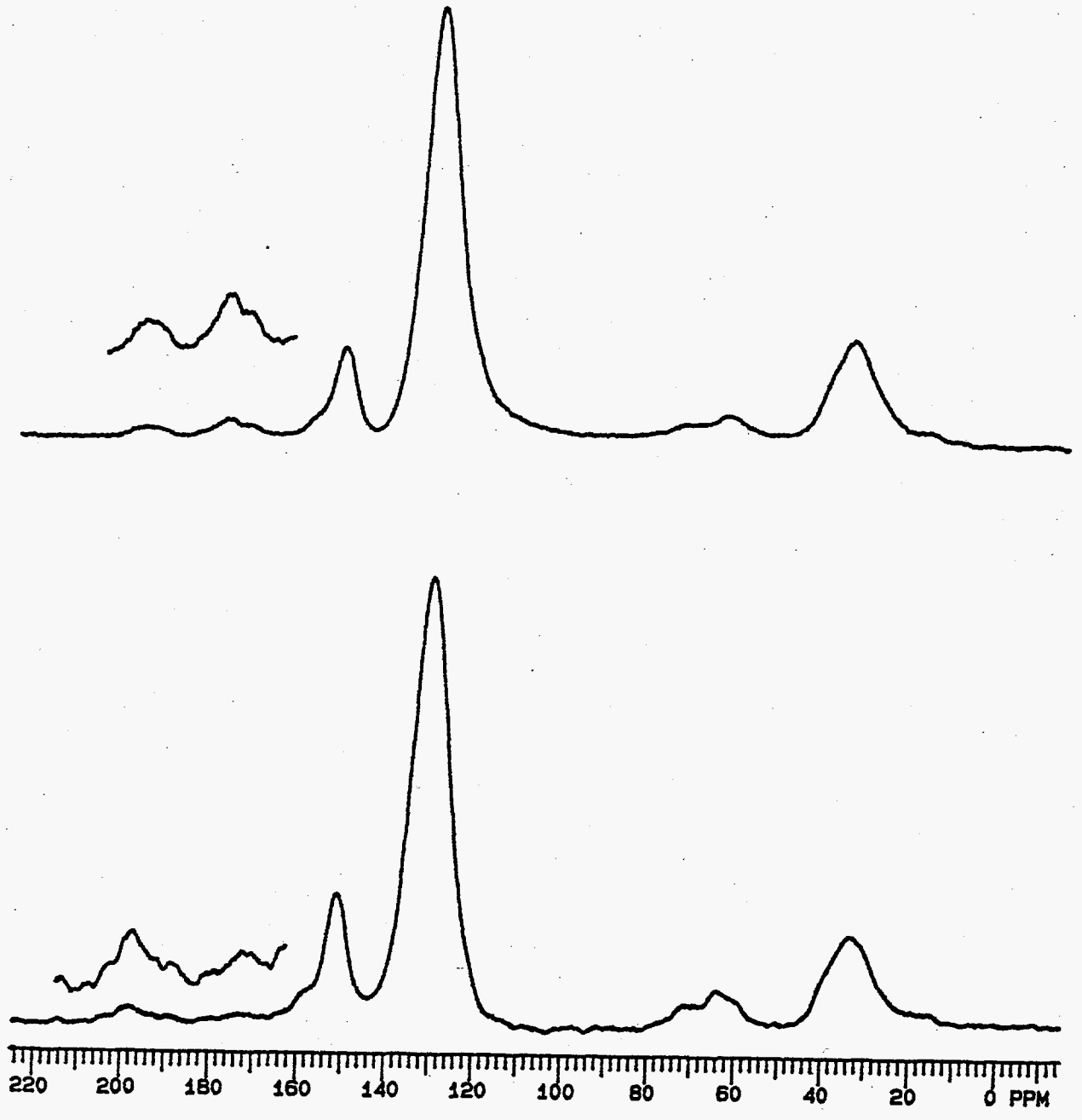

Figure 4-29. ^{13}C NMR Spectra of CS-100 Resin Obtained at 12 kHz MAS for Conditions of Gamma Irradiation (5×10^8 R) with Static NCAW Waste Simulant (top) Compared to Standard CS-100 Resin (bottom)

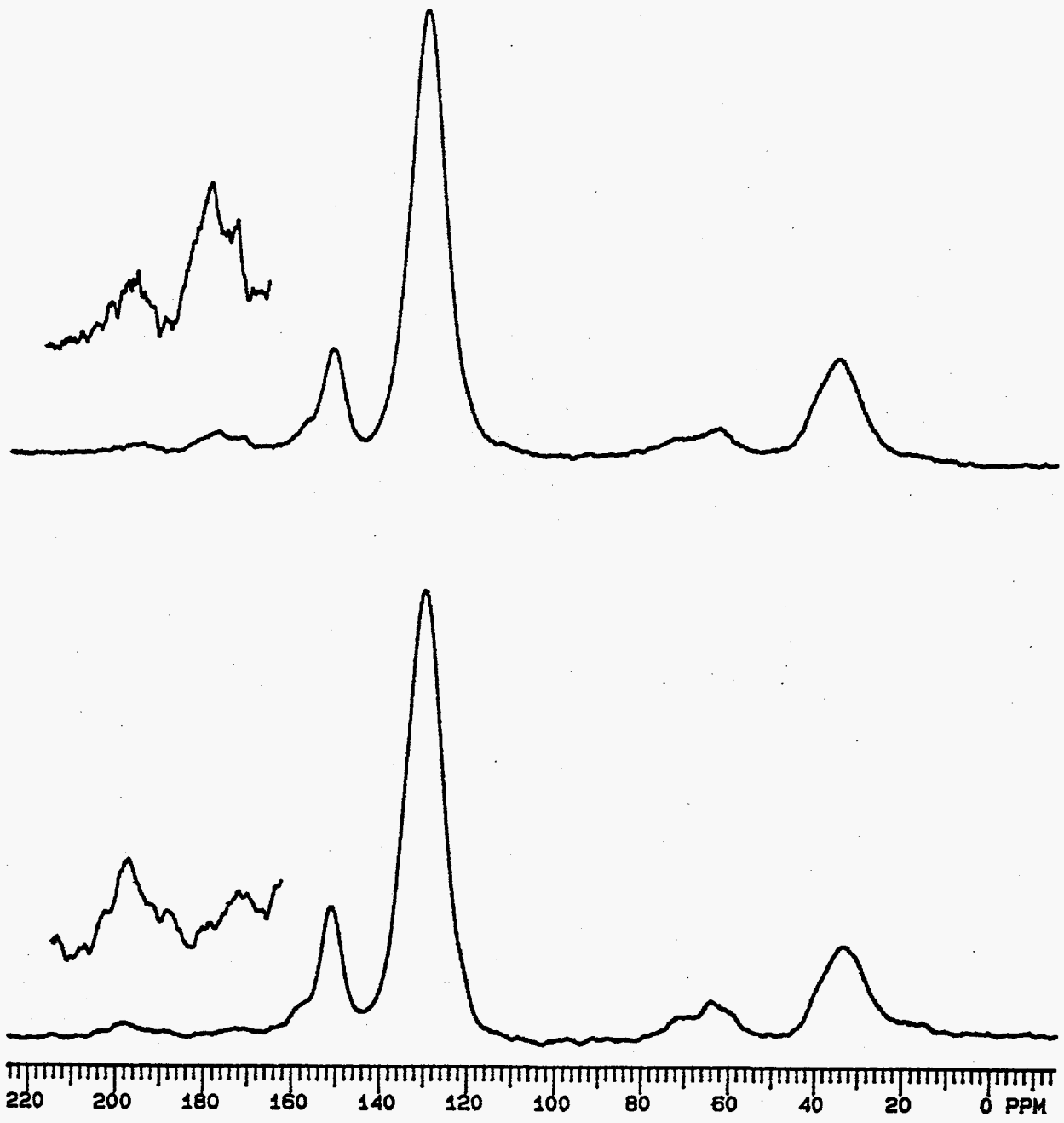

Figure 4-30. ^{13}C NMR Spectra of CS-100 Resin Obtained at 12 kHz MAS for Conditions of No Gamma Irradiation with Static NCAW Waste Simulant (top) Compared to Standard CS-100 Resin (bottom)

4.5.1 Gas Generation for Cation Exchange Resin and NCAW Supernate

The gas generation of the static tests were monitored by pressure increases within the vessel and mass spectral analysis if the gas products accumulated throughout the duration of the experiment. In all cases the thermal generation of gases was negligible. G values calculated for the formation of gaseous products as a function of gamma dose for the R-F resin and CS-100 resin tests as well as the NCAW only irradiation test are presented in Table 4.11.

Table 4.11. G Values for the Production of Gases for Several NCAW-Simulated Waste Supernate Solutions Containing R-F Resins, CS-100 Resin, and NCAW Supernate Only

	G Values (molecules/100 eV)				
Sample	**$G(H_2)$**	**$G(N_2)$**	**$G(O_2)$**	**$G(N_2O)$**	**Gamma Dose Rate**
R-F resin BSC-187	1.65×10^{-2}	3.94×10^{-3}	3.30×10^{-5}	3.76×10^{-3}	2.1×10^{5} R/h
R-F resin BSC-210	1.30×10^{-2}	3.30×10^{-3}	3.53×10^{-5}	3.18×10^{-3}	$2.2.x\ 10^{5}$ R/h
CS-100	1.05×10^{-2}	3.55×10^{-3}	1.98×10^{-3}	3.31×10^{-3}	2.7×10^{5} R/h
NCAW	1.59×10^{-2}	1.47×10^{-3}	7.54×10^{-2}	4.41×10^{-5}	1.5×10^{5} R/h

Gas generation data for static testing of the BSC-187 and BSC-210 R-F resin and CS-100 resin immersed in NCAW supernate is summarized in Figures 4-31 to 4-33. For these tests, hydrogen was the most abundant gas produced and had the highest measured G value. Nitrogen and nitrous oxide were produced in approximately equal quantities.

Oxygen was not produced at a significant level for the system containing R-F resin, in contrast to the similar system containing CS-100 resin. Figure 4-34 contains the oxygen gas generation with time for these resins under irradiation conditions. $G(O_2)$ for the BSC-187 and BSC-210 R-F resin ($3.3x10^{-5}$ and $3.5x10^{-5}$ respectively) is approximately two orders of magnitude lower than $G(O_2)$ for CS-100 ($3.3x10^{-3}$). This difference in oxygen production can be attributed to the higher reactivity of the activated resorcinol functionality of the R-F resin (compared to the phenolic function of CS-100) towards the hydroxy radical formed in the radiolysis of the resin-NCAW system. The reaction and capture of the hydroxy radical prevents its eventual formation of molecular oxygen by other reaction pathways.

To assess the amount of gas generation induced by the presence of added organic resin, we irradiated NCAW supernate without added resin material. Figure 4-35 contains data for the moles of gases generated during radiolysis of the NCAW supernate. The $G(O_2)$ for the production of oxygen (Table 4.11) is higher than either of the experiments containing organic resins. Nitrogen and nitrous oxide are observed as minor products and at lower yields than for the parallel experiments containing organic resins. The source of these products is from the reduction of nitrite and nitrate in solution.

Hydrogen and oxygen are expected radiolytic products resulting from the initial homolysis of the O-H bond of water forming H• and OH• radicals. The molecular decomposition products of pure water have a stoichiometric ratio of H_2 and O_2. In the aqueous system containing organic resins (R-F and CS-100), the radiolytic hydrogen to oxygen ratio is much higher than that for the NCAW solution alone, due to the presence of a source hydrocarbon material which is effective at scavenging OH• to reform water.

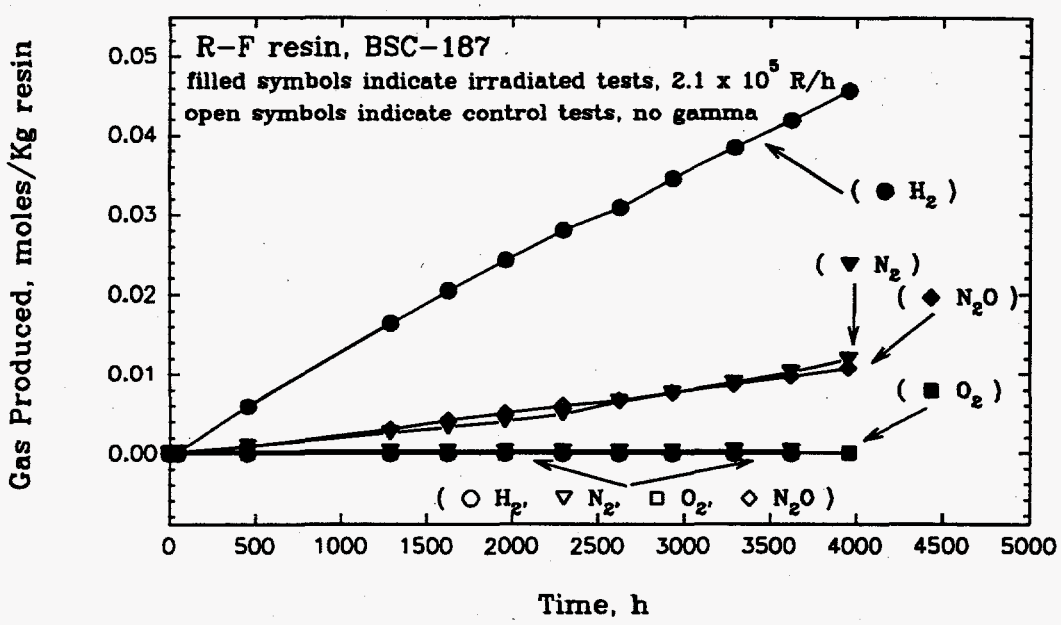

Figure 4-31. Gas Generation from BSC-187 R-F Resin in NCAW Supernate Under Gamma Irradiation and Control Conditions

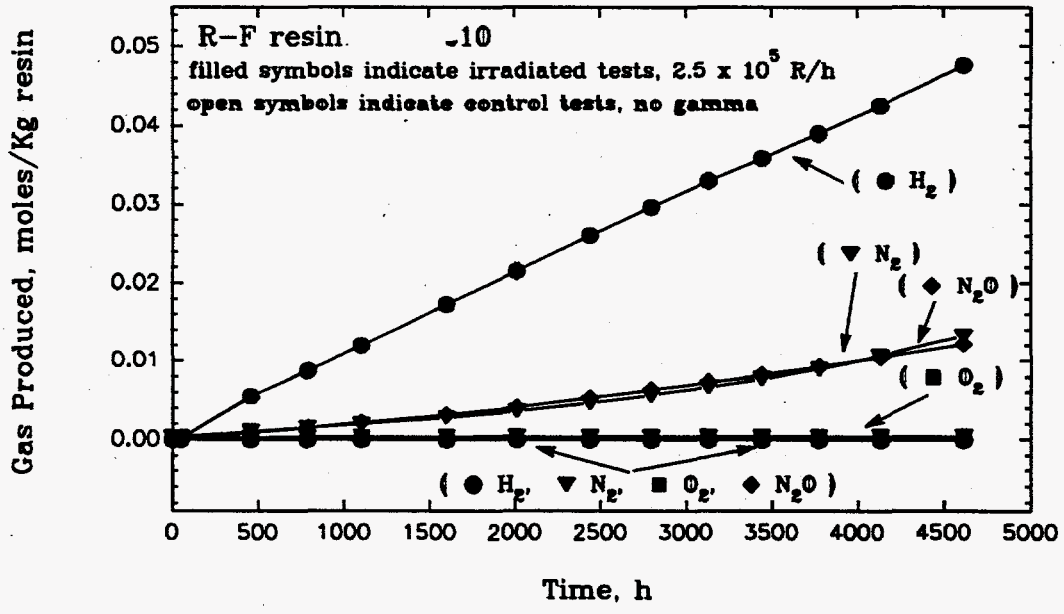

Figure 4-32. Gas Generation from BSC-210 R-F Resin in NCAW Supernate Under Gamma Irradiation and Control Conditions

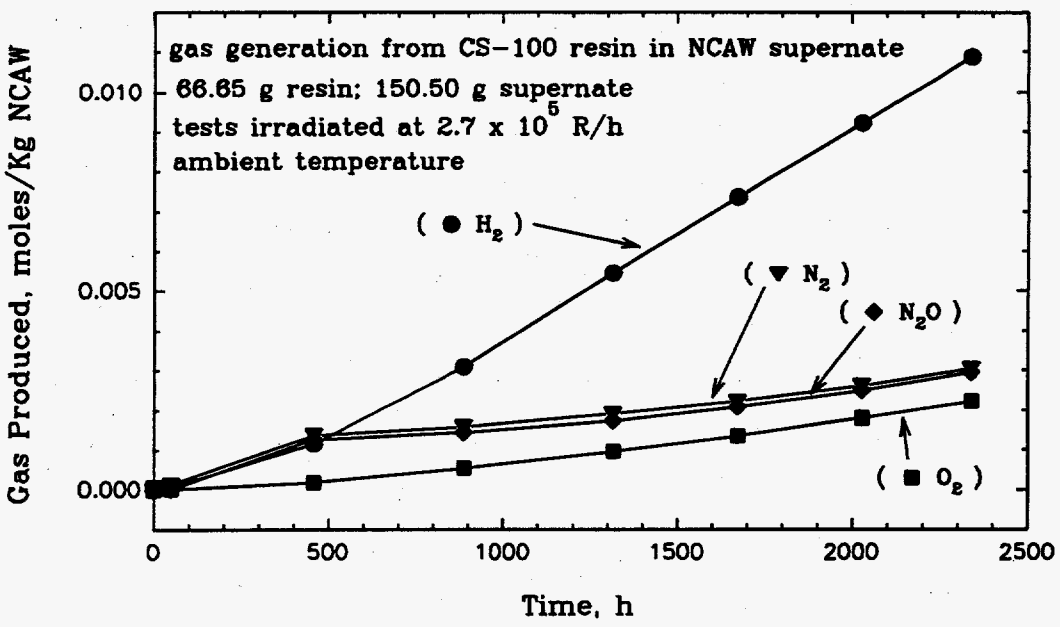

Figure 4-33. Gas Generation from CS-100 Resin in NCAW Supernate Under Gamma Irradiation and Control Conditions

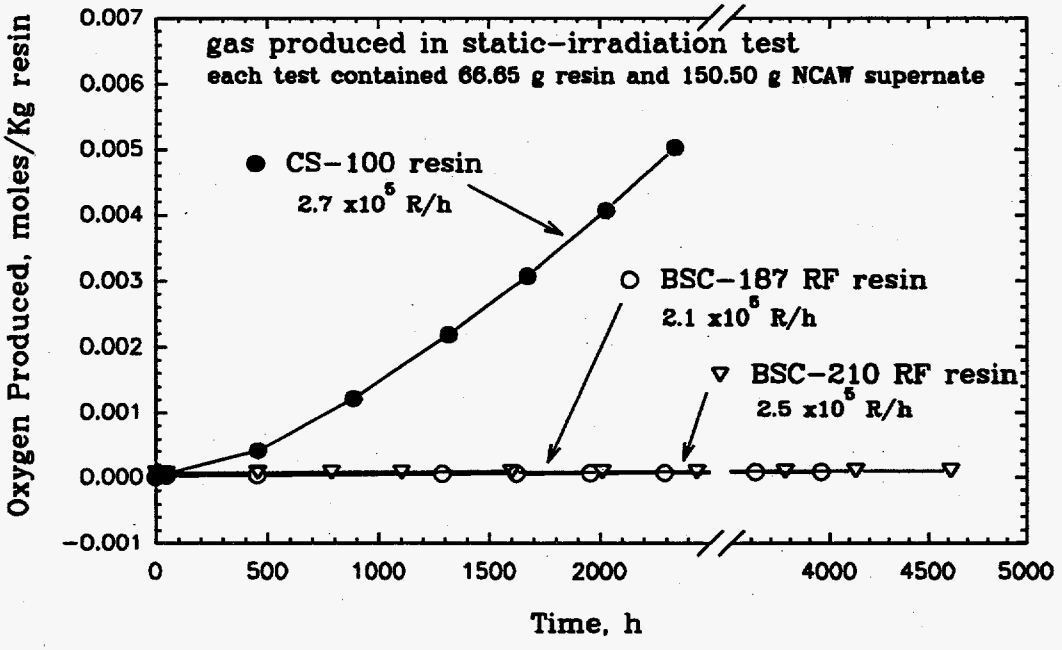

Figure 4-34. Comparison of Oxygen Gas Generation from CS-100, BSC-187, and BSC-210 Resins in NCAW Supernate Under Gamma Irradiation Conditions

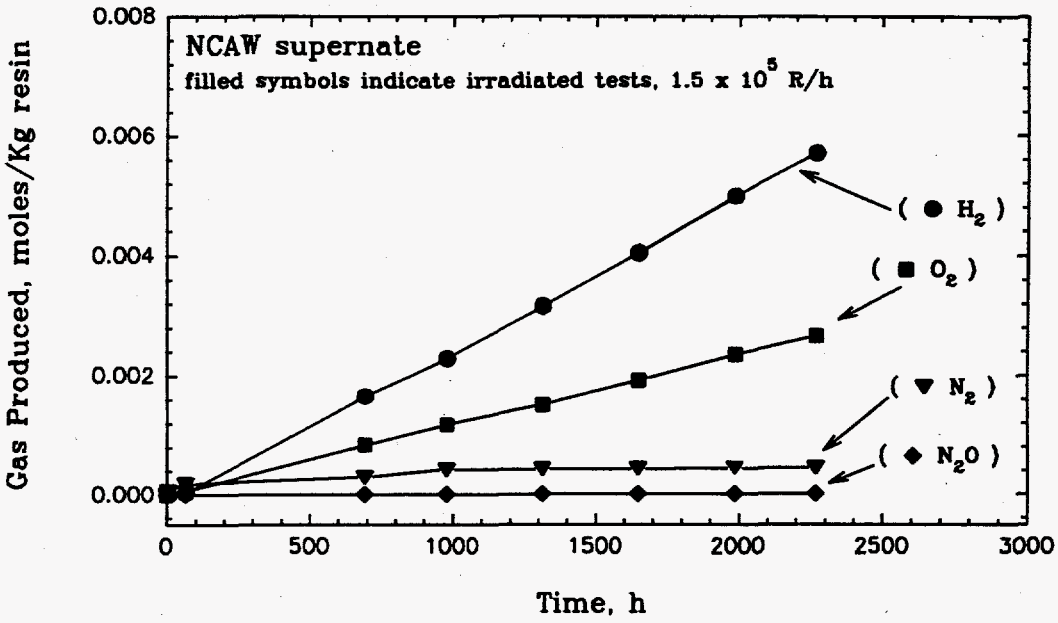

Figure 4-35. Gas Generation from NCAW Supernate Under Gamma Irradiation

This prevents its recombination with another hydroxyl radical to form H_2O_2 and eventually its molecular decomposition product, O_2. The H• radical can react with a like radical (H•) or directly with the hydrocarbon resin to form H_2. Nitrogen and nitrous oxide are both observed molecular decomposition products in all of the irradiated static tests of NCAW simulated waste, whether organic resins are present or not. The nitrogen containing products are produced in a higher yield for the systems with organic resins than for the NCAW system only. In the system with added organic resins (R-F and CS-100), the resins themselves are the primary thermodynamic source of reductant. These nitrogen containing gases have been produced in similar systems containing nitrite and nitrate with organic carbon present [19, 20]. Since the resins tested and the NCAW supernate do not contain organic nitrogen, the source of nitrogen in N_2 and N_2O must be from nitrate and nitrite from the NCAW waste simulant. Under reducing conditions in basic solution, nitrate and nitrite have been shown to be unstable toward reduction forming the gaseous products N_2, N_2O and NH_3 [21]. Although ammonia has not been observed in this system, the organic is believed to be acting as the reducing agent toward nitrite and nitrate to form nitrogen and nitrous oxide. Even in the NCAW system with no added organic resin, some nitrogen and nitrous oxide is formed, presumably from the direct reduction of nitrite and nitrate ions by H• radical.

4.5.2 Corrosion

Stainless steel corrosion coupons were placed in the test vessels during resin stability testing to assess steel corrosion under test conditions. Coupons were placed within the test vessels containing the CS-100 and BSC-187 R-F resins. Corrosion coupons were used in the flow and static tests, in both the control and irradiated tests. The stainless steel coupons were machined from a single sheet of 304L stainless (1.2 mm thick) and uniquely stamped for identification. Standard methods of the American Society for Testing and Materials (ASTM) and National Association for Corrosion Engineers (NACE) were employed for cleaning and weighing the corrosion coupons prior to testing. The average surface area of each coupon was approximately 11 cm^2. Three coupons were used per test vessel, and evenly spaced within the resin. The total steel surface area in each test was approximately 200 cm^2/Kg resin.

Corrosion coupons were left within the resin during each resin test, flow with and without gamma irradiation, and static with and without gamma irradiation. The total length of corrosion test for each experiment was approximately 2400 h in the CS-100 resin test and approximately 4000h in the BSC-187 R-F resin tests. Corrosion rates based on linearized corrosion rates were calculated at the conclusion of the test. Table 4.12 contains corrosion data for both the CS-100 and R-F resin tests.

The corrosion data (Table 4.12) shows that for the CS-100 and R-F resin the measured corrosion rate is extremely small. The negative values obtained for the CS-100 tests indicate was due to a precipitation film that could not be removed by the washing procedure prior to measuring the final mass of the test coupon following the test.

Table 4-12. Coupon Corrosion Tests Summary for CS-100 and R-F Resin (Test coupons were inserted within resin within test vessels during irradiation and control tests)

Test Conditions	Corrosion Rate, MPY	Mass Loss, wt%
	CS-100 Resin Test Coupons	
irradiated - flow	0.0045 ± 0.002	0.0048 ± 0.002
irradiated - static	-0.0055 ± 0.01	-0.0069 ± 0.01
non-irradiated - flow	-0.00067 ± 0.001	-0.00068 ± 0.001
non-irradiated - static	-0.00067 ± 0.001	-0.00068 ± 0.001
	R-F Resin Test Coupons	
irradiated - flow	0.0042 ± 0.001	0.0093 ± 0.003
irradiated - static	0.0020 ± 0.001	0.0039 ± 0.002
non-irradiated - flow	0.0019 ± 0.00002	0.00039 ± 0.00005
non-irradiated - static	0.0020 ± 0.00006	0.0039 ± 0.00005
blank coupons		0.0027 ± 0.003

A precipitation coating formed on the test coupons for the static-irradiastion test for both the CS-100 and R-F resin tests. For the static-non-irradiation test, no coating layer or visible corrosion was observed. Due to the insignificant mass loss of the test coupons (Table 4.12), we believe the observed coating is a precipitated layer onto the steel coupon rather than a corrosion product, due to its appearance and ability to peel away from the coupon exposing an untarnished surface of the test coupon. Initial analysis of the coating layer from the static-irradiated corrosion coupons by infrared techniques indicates that the coating is not composed of an organic hydrocarbon material.

For both experiments, using CS-100 and R-F resin, for the flow-irradiated and the flow non-irradiated tests, there was very little observable difference in appearance of the coupons from before to after testing. The flow-irradiated corrosion coupons show slight discoloration, while the flow non-irradiated coupons appear new. The small to negligible mass loss observed in the corrosion studies indicate that corrosion of the 304L stainless steel is not a problem in the flow tests under control or irradiated conditions.

In the static-irradiated test (for both the CS-100 and R-F resins) there was a coating layer precipitated onto the corrosion coupon, but in the flow-irradiated system, there is no evidence for the formation of the coating

layer. The coating material on the static-irradiated tests must originate from the radiolysis of the NCAW waste simulant, since there is no evidence of this coating behavior in the static non-irradiated tests. The reaction rate of the irradiation produced coating material must be slow in order to allow the column feed rate of approximately 0.5 CV/h in the flow system to be able to sweep out the coating material before it had time to react with, and produce a coating on the coupons.

Solubility properties of the coating material may be an alternative explanation for the difference between the observed coating on the static-irradiated corrosion coupons, and lack of coated material on the flow-irradiated coupons. The solubility of the coating material may be exceeded in the static test where the irradiation produced coating material is continually increasing within solution. In the flow-irradiated solution, the irradiation produced coating material is continually diluted by fresh NCAW feed (0.5 CV/h) and therefore does not build up to a concentration high enough to exceed the solubility limit.

Consistent with the observations for the corrosion coupons, a similar coating product has been observed to form on the stainless steel mesh, grid with spacer pins, and interior surface of the test vessel in the static-irradiated test, but not for the identical parts in the static non-irradiated tests. No coating material was observed on the stainless steel mesh, grid with spacer pins, or stainless steel O-ring, or vessel surface on the flow-irradiated or flow non-irradiated tests in agreement with the corrosion coupon results above.

5.0 Conclusion/Recommendations

This chapter presents the main conclusions and observations presented in this report along with some recommendations. The information is broken down into the following subject areas: chemical structure, ion-exchange performance, and chemical and radiolytic stability.

Chemical Structure

- The primary structural unit of R-F resin is a 1,2,3,4-tetrasubstituted resorcinol ring. Solid-state ^{13}C CP-MAS NMR spectra for ^{13}C label-enhanced resin shows the presence of two non-equivalent methylene group carbons as expected for a 1,2,3,4-tetrasubstituted resorcinol ring. FTIR structural analysis for R-F resin shows a primary band at 802 cm^{-1} corresponding to aromatic out of plane C-H bending which is indicative of the 1,2,3,4-tetrasubstituted ring pattern for the resorcinol unit. FTIR analysis also indicates the likely presence of some 1,2,4,5-tetrasubstituted and/or 1,2,4-trisubstituted resorcinol ring units which comprise 15% or less of the polymer structure by presence of a medium-weak band at 865 cm^{-1}. Elemental analyses for R-F resin in both the acid and potassium forms is consistent with a 1,2,3,4-tetrasubstituted ring structure. For the potassium form, one unit of water is likely associated with each potassium ion. Elemental analyses for the sodium and cesium forms of the R-F resin (BSC-187) also are consistent with this structure.

- The primary structural unit of CS-100, a P-F resin, consists of a 1,2,4-trisubstituted phenol ring. Solid-state ^{13}C CP-MAS NMR spectra for CS-100 shows the presence of significant amounts of ether groups in the resin, such that the resin is constructed primarily from two groups as shown in Figure 4-17. One of the groups is no longer a phenol, but rather has an ether functionality in place of the hydroxyl and comprises about 54.8% of the resin; the other group is the 1,2,4-trisubstituted phenol group, present in about 45.2% of the resin (based on integration of Bloch Decay spectra). This probably means that this resin has less than half of the theoretical ion-exchange capacity because the hydroxyl groups are converted into ether groups during synthesis of the resin. The manufacturer's data sheets show that CS-100 has a polymer modifier added to it, *p*-toluic acid, but there is no indication of its presence in the resin; ^{13}C spectra do not exhibit carboxylate or carboxylic acid resonances. The toluic acid cannot crosslink effectively and may simply be washed out of the polymer matrix on final treatment of the product for delivery. FTIR analysis of CS-100 is consistent with the 1,2,4-trisubstituted ring pattern of the phenolic ring with bands appearing at 799 (s) and 876 (m) cm^{-1} as the aromatic out of plane C-H deformation bands. Elemental analyses for this resin give results that are slightly low on C and H content which probably indicates the presence of more oxygen incorporated into the resin from chemical degradation during or after synthesis.

Ion-Exchange Performance

- Curing temperatures for R-F resin should be kept at around 105 °C and should not exceed 130 °C. Curing of resin below this temperature results in insufficient curing and crosslinking of the resin. The result is that the ion-exchange performance of the resin is reduced because the lower crosslinked resin has much lower selectivity for cesium ion. An upper limit of 130 °C for curing

temperature is suggested because significant organic decomposition of the resin is observed at 135 °C in the TGA/IR analysis performed on the resin. Also, analysis of K_d's for R-F resin cured at temperatures above 135 °C in an inert helium atmosphere also show drastic reduction of cesium K_d's. The lower K_d's result from oxidation of the resin.

- The optimal particle size for the R-F resin to be used in an ion-exchange process is in the range of 20-50 mesh sized particles. Particles larger than 20 mesh give lower K_d's because ion exchange is diffusion limited in the larger particles. For particles smaller than 50 mesh, the surface area of the resin is increased as the particles become smaller, so ion-exchange should increase as well; however, the greater surface area presented is also more easily oxidized or otherwise chemically degraded with concomitant loss of ion-exchange sites.

- Synthesis of macroreticular R-F resin forms will be problematic and is not necessarily desirable. Some R-F resin derivatives which were hoped to be macroreticular were prepared in an effort to increase surface areas and selectivities for cesium. Macroreticular resins have much higher surface area because of the presence of large pore structures throughout the resin. However, the surface areas are also subject to oxidation, with subsequent loss of performance for the resin. Another important point in this regard is that selectivity for cesium for R-F resin is associated with the swelling characteristics of the resin. A macroreticular resin would be more rigid and would swell less, hence the selectivity for cesium would be reduced.

- Preparation of R-F resin under anaerobic conditions will not significantly increase the performance of the resin. A batch of R-F resin was prepared under anaerobic conditions and gave a slightly lower value of K_d than batches prepared under normal atmospheric conditions. The reason that the K_d was lower probably arose because it was more difficult to drive water off during the curing process resulting in a resin with slightly lower crosslinking. Preparation of the resin under anaerobic conditions has not been optimized, however.

- Use of KOH in the preparation of R-F resin probably is unnecessary and has little effect on the K_d of the resin produced. A batch of R-F resin was prepared using LiOH and this gave a resin with good performance, only slightly lower than that prepared with KOH. Bibler has claimed a templating effect is important in creating ion-exchange sites of the correct size for cesium as the reason for using KOH rather than NaOH or other alkali hydroxides during synthesis of R-F resin. However, the ion-exchange performance and the structural characteristics of the resin were essentially identical for both KOH and LiOH synthesized resins. Indeed, because potassium ion is known to compete with cesium for ion-exchange sites, this may be a reason for not using KOH for the synthesis of the resin. Further studies will be needed to address this question of templating effect more clearly, however.

Chemical and Radiolytic Stability

- R-F resin undergoes chemical degradation which destroys ion-exchange sites, thus lowering the performance of the resin. ^{13}C CP-MAS NMR show conclusively that the R-F resin degrades to give ketone, quinone, and ether functionaliites. Resonances for these functional groups appear in the spectra after exposure of the resin to air and pure oxygen in a variety of media, while simultaneously, the resonances of the hydroxyl aromatic carbons centered around 150 ppm lower in relative intensity. Thus, the ion-exchange sites (hydroxyl functionality) are likely being

converted into quinone groups and the ion-exchange sites are destroyed. Dry resin seems to be fairly stable and probably only surface oxidation is occurring as the carbon spectra don't change significantly over a long period of time. Some of the issues which need to be addressed are which form of the resin is best for storage (e.g. potassium form or hydrogen form), and determination of the chemical pathway for chemical degradation of the resin. Clearly, ^{13}C CP-MAS NMR is a useful method for monitoring resin quality as demonstrated by all the studies into structure and chemical degradation of the resin.

6.0 References

1. Helfferich, F. *Ion Exchange*; McGraw-Hill: New York, **1962**, p. 121.

2. a) Pedersen, C.J. *J. Am. Chem. Soc.* **1987**, *89*, p. 7017.
   b) Izatt, R.M.; Bradshaw, J.S.; Nielsen, S.A.; Lamb, J.D.; Christensen, J.J.; Sen, D. *Chem. Rev.* **1986**, *86*, p. 271.
   c) Hayashita, T.; Goo, M.; Lee, J.C.; Kim, J.S.; Krzykawski, J.; Bartsch, R.A. *Anal. Chem.* **1990**, *62*, p. 2283.

3. Dressler, H. *Resorcinol: Its Uses and Derivatives*; Plenum Press: New York, **1994**, p. 6.

4. Bibler, J.P.; Wallace, R.M.; Bray, L.A. "Testing a New Cesium-Specific Ion Exchange Resin for Decontamination of Alkaline High-Activity Waste," *Proceedings of Waste Management '90, Tucson, Arizona*, **1990**, *2*, p. 747.

5. Kurath, D.E.; Bray, L.A.; Brooks, K.P.; Brown, G.N.; Bryan, S.A.; Carlson, C.D.; Deschane, J.R.; Elovich, R.J.; Kim, A.Y. *Experimental Data and Analysis to Support Design of an Ion-Exchange Process for the Treatment of Hanford Tank Waste Supernatant Liquids*; **1994**, PNL-10187, Prepared by Pacific Northwest Laboratory for Westinghouse Hanford Company, Richland, Washington.

6. Samanta, S.K.; Ramaswamy, M.; Misra, B.M. "Studies on Cesium Uptake by Phenolic Resins," *Sep. Sci. Tech*, **1992**, *27(2)*, p. 255.

7. See Reference #1, p. 100-125.

8. Marsh, S.F.; Svitra, Z.V.; Bowen, S.M. *Distributions of 14 Elements on 63 Absorbers from Three Simulant Solutions (Acid-Dissolved Sludge, Acidified Supernate, and Alkaline Supernate) for Hanford HLW Tank 102-SY*; **1994**, LA-12654, Rev., Los Alamos National Laboratory, Los Alamos, New Mexico.

9. "Cesium-Specific Phenolic Ion Exchange Resin," PCT Int. Appl WO 91,009,891 (11 July 1991; J.P. Bibler and R.M. Wallace to the U.S. Department of Energy); *C.A., 115*, 234200 **(1991)**.

10. Pennington, L.D.; Williams, M.B. *Ind. Eng. Chem.* **1959**, *6*, 759.

11. Bray, L.A. PNL Test Procedure. "Determination of Batch Sorption Ratios for Ion-Exchange Materials Using Radionuclide Tracer Techniques," **1989**, WTC-006-21-1.

12. Brunauer, S.; Emmett, P.H.; Teller, E.J. *J. Am. Chem. Soc.* **1938**, *60*, 309.

13. Bunker, B.C. *Evaluation of Inorganic Ion Exchangers for Removal of Cesium From Tank Wastes*; **1994**, TWRSPP-94-085, prepared by Pacific Northwest Laboratory for Westinghouse Hanford Company, Richland, Washington.

14. a) Pekala, R.W.; Kong, F.M. *Polym. Prpts.* **1989**, *30*, p. 221.
b) Pekala, R.W. *J. Mater. Sci.* **1989**, *24*, p. 3221.

15. Aoyama, Y., Tanaka, Y.; Sugahara, S. *J. Am. Chem. Soc.* **1989**, *111*, p. 5397.

16. Kim, M.G.; Amos, L.W.; Barnes, E.E. *J. Polym. Sci., Part A: Polym. Chem.* **1993**, *31(7)*, 1871.

17. a) Werstler, D.W. *Polymer* **1986**, *27*, 757.
b) Sebenik, A.; Osredkar, U.; Vizovisek, I. *Polymer* **1981**, *22*, 804.

18. See Reference #3, p. 418.

19. Bryan, S.A., L.R. Pederson, R.D. Scheele, J.L. Ryan, and J.M. Tingey. **1992**. *Slurry Growth, Gas Retention and Flammable Gas Generation by Hanford Radioactive Waste Tanks: Synthetic Waste Studies, FY-1991*. PNL-8169, Pacific Northwest Laboratory, Richland, Washington.

20. Bryan, S.A. and L.R. Pederson. **1994**. *Composition, Preparation, and Gas Generation Results from Simulated Wastes of Tank 241-SY-101*. PNL-10075, Pacific Northwest Laboratory, Richland, Washington.

21. Pourbaix, M. **1974**. *Atlas of Electrochemical Equilibria in Aqueous Solutions*. National Association of Corrosion Engineers, Houston, Texas, pp. 493-503.

Distribution

No. of Copies

Offsite

2 DOE/Office of Scientific and Technical Information
P.O. Box 62
Oak Ridge, TN 37831

J. P. Bibler
MS 773-A
Westinghouse Savannah River Laboratory
Aiken, SC 29808

J. M. Birmingham
Boulder Scientific Company
598 Third Street
Mead, CO 80542

Dr. Teresa Fryberger
U.S. Department of Energy
EM-532 Cloverleaf
19901 Germantown Road
Germantown, MD 20874

Phil McGinnis
Oak Ridge National Laboratory
Martin Marietta Energy Systems, Inc.
P.O. Box 2008
Oak Ridge, TN 37831

R. D. Hunt
Oak Ridge National Laboratory
Martin Marietta Energy Systems, Inc.
P.O. Box 2008
Oak Ridge, TN 37831

No. of Copies

Edward I. Rizkalla, PE
EM-361, Trevion II
U.S. Department of Energy
1000 Independence Ave. S.W.
Washington, D.C. 20585

Dennis Wynne
EM-361, Trevion II
U.S. Department of Energy
1000 Independence Ave. S.W.
Washington, D.C. 20585

Onsite

3 **DOE Richland Operations Office**

S.T. Burnum	S7-53
P.T. Furlong	G3-20
L.S. Waldorf	K6-51

13 **Westinghouse Hanford Company**

J.N Appel	G3-21
L.D. Arnold	B2-35
S.A. Barker	R2-11
K.M. Eager	H5-27
R.R. Gadd	B4-49
K.A. Gasper	G3-21
R.A. Kirkbride	H5-27
M.J. Klem	H5-27
R.M. Orme	H5-27
D.L. Penwell	H5-27
I.E. Reep	G3-21
J.P. Sloughter	H5-27
D.J. Washenfelder	H5-27

No. of Copies

64 **Pacific Northwest Laboratory**

D.B. Anderson		P7-41
E.G. Baker		P8-38
L.A. Bray		P7-25
K.P. Brooks		P7-43
G.N. Brown		P7-25
S.A. Bryan		P7-25
J.L. Buelt		P7-41
B.C. Bunker		K2-45
L.D. Carlson		P7-25
J.A. Franz	(10)	K2-38
J.W. Grate		K2-12
R.T. Hallen		P8-38
B.P. Hay		K9-77
L.K. Holton		P7-43
T.L. Hubler	(20)	P8-38
A.Y. Kim		K2-44
W.L. Kuhn		K2-21
D.E.Kurath		P7-43
J.P. LaFemina		K2-25
J.C. Linehan		K2-38
N.J. Lombardo		K9-91
G.J. Lumetta		P7-25
E.V. Morrey		P7-19
S.J. Ortiz		P8-38
J.M. Perez		P7-41
B.M. Rapko		P7-25
B.A. Reynolds		P7-19
L.J. Sealock		K2-10
W.J. Shaw		K2-44
T.L. Stewart		K9-91
J.M. Tingey		P7-25
Technical Report Files		(5)